



## Research article

## Understanding the aqueous chemistry of quinoline and the diazanaphthalenes: insight from DFT study

Obieze C. Enudi<sup>\*</sup>, Hitler Louis<sup>\*\*</sup>, Moses M. Edim, John A. Agwupuye, Francis O. Ekpen, Emmanuel A. Bisong, Patrick M. Utsu

Computational and Bio-Simulation Research Group, University of Calabar, Calabar, Nigeria

## ARTICLE INFO

## Keywords:

Diazanaphthalenes  
Quinolone  
Aqueous  
DFT  
Adsorption

## ABSTRACT

The inter-fragment interactions at various binding sites and the overall cluster stability of quinolone (QNOL), cinnoline (CNOL), quinazoline (QNAZ), and quinoxaline (QNOX) complexes with H<sub>2</sub>O were studied using the density functional theory (DFT) approach. The adsorption and H-bond binding energies, and the energy decomposition mechanism was considered to determine the relative stabilization status of the studied clusters. Scanning tunneling microscopy (STM), natural bonding orbitals (NBO) and charge decomposition were studied to expose the electronic distribution and interaction between fragments. The feasibility of formations of the various complexes were also studied by considering their thermodynamic properties. Results from adsorption studies confirmed the actual adsorption of H<sub>2</sub>O molecules on the various binding sites studied, with QNOX clusters exhibiting the best adsorptions. Charge decomposition analysis (CDA) revealed significant charge transfer from substrate to H<sub>2</sub>O fragment in most complexes, except in QNOL, CNOL and QNAZ clusters with H<sub>2</sub>O at binding position 4, where much charges are back-donated to substrate. The O—H inter-fragment bonds was discovered to be stronger than counterpart N—H bonds in the complexes, whilst polarity indices confirmed N—H as more polar covalent than O—H bonds. Thermodynamic considerations revealed that the formation process of all studied complexes are endothermic (+ve  $\Delta H_f$ ) and non-spontaneous (+ve  $\Delta G_f$ ).

## 1. Introduction

The agrochemical, pharmaceutical, corrosion and veterinary industries are few of the vast application fields for heterocyclic compounds (HCs) [1, 2, 3, 4]. In order to expand the domain of consumption of heterocyclic compounds and its derivatives, much energy has been channeled into the development [2], synthesis [2, 3, 4, 5, 6, 7, 8, 9, 10, 11, 12] and interaction studies of these compounds [13, 14, 15] in various solvent systems. Many important organic-based chemical industries utilizes HCs as their feedstock, for special and multipurpose chemicals manufacture. They have been used in corrosion inhibitor products [10], developers, sanitizers [3], etc. It is also noteworthy that many enzymes and living tissues contain HCs in their backbone [1]. Heterocyclic compounds are cyclic compounds having at least two kinds of atoms in its ring skeleton (mostly carbon and non-metals like Nitrogen, Sulphur, Oxygen, etc.). HCs are classified as aromatic or non-aromatic, depending on the electronic composition of the rings [1].

Aromatic HCs must obey the general *Huckels* rule, which states that any aromatic compound must have  $4n + 2$  amount of  $\pi$  electrons in its ring system, examples are furan, pyridine, thiophene, quinoline, etc. The non-aromatic heterocycles are those that don't exhibit the aromatic ring structure, e.g., tetrahydrofuran, thiirane, thietane, etc. Quinoline, cinnoline, quinazoline and quinoxaline are aromatic HCs of nitrogen [1, 16, 17, 18]. They are generally obtained structurally by doping naphthalene with nitrogen atom(s). A mono doping of naphthalene with N at position 1 yields a quinolone molecule [19, 20]. While cinnoline, quinazoline and quinoxaline are derived via di-doping of naphthalene with N atoms at positions 1 and 2, 1 and 3, and 1 and 4, respectively [21, 22, 23, 24]. The inclusion of N atoms in the backbone of naphthalene chemically alters the electronic make-up, hence the emergence of new properties of interest.

Diazanaphthalenes are building blocks for many medical and structural valuable chemicals. Some quinoline and cinnoline derivatives for instance are recently explored in the medical industry, many are under

<sup>\*</sup> Corresponding<sup>\*\*</sup> CorrespondingE-mail addresses: [enudij@gmail.com](mailto:enudij@gmail.com) (O.C. Enudi), [louismuzong@gmail.com](mailto:louismuzong@gmail.com) (H. Louis).

clinical test for their antifungal, antimalarial, anti-inflammatory, analgesic, antitumor, etc., activities [25, 26, 27, 28].

The density functional theory (DFT) method of analysis, which exposes the electronic compositions, hence properties, is an important approach to the study of interacting molecules in conjugate systems [29], unlike when molecules interact, adhesive bonds are formed. So, for an appreciable understanding of the system, the nature and energies of the interaction bonds, and the charge transfers are required [30]. Also the thermodynamic properties ( $\Delta H$ ,  $\Delta S$  and  $\Delta G$ ) of the process is demanded [31].

Relevant DFT works have been conducted on the activities of quinoline and other heterocycle derivatives [32, 33]; derivatives of quinoline tested as anti-tuberculosis agents showed positive results, pending in-vitro and in-vivo confirmation test [32]. Also, the anti-corrosion properties of some heterocycles are reported [34, 35]. In decision making of the applicability of molecules in a specific field, the interaction properties of the molecule and intended system composition is crucial. Hence, the aqueous chemistry of valuable active materials is imperative. Several DFT researches have been reported on the interactions of H<sub>2</sub>O with cluster systems [36, 37, 38, 39, 40, 41].

Understanding the aqueous chemistry of quinoline and the diazaphthalenes will further explain their pharmacodynamics and pharmacokinetics in biological systems [42, 43]. Those of their derivatives can also be predicted considering the groups accommodated. This current study will expose in details, the adsorption properties of quinolone and some selected diazaphthalene compounds (cinnoline, quinazoline and quinoxaline), which will be achieved through a systematic merge of H<sub>2</sub>O molecule on different binding sites on the activated ring of the pseudo-naphthalene compounds, to form a complex. The hydrogen bond characteristics are discussed in detail, the adsorption energies, significance and applicability are also exhaustively treated. Furthermore, the thermodynamics of formation of the substrate + H<sub>2</sub>O complexes are studied. The various studied complexes are titled in Table 1., for easy discussion and reference.

## 2. Computational methods

For the fragment-fragment interaction studies of various titled complexes of water with quinoline and some selected di-azanaphthalene moieties, the Gaussian 09 software [44] coupled with Gauss-view interface was employed for the ground state optimizations, frequency calculations, natural bonding orbitals (NBO) analysis and surfaces and contour plotting, employing the DFT/B3LYP method and 631-G (d) basis set [45]. The basis set; 631-G(d) is relatively good for energy determinations, a heavy atom polarization term, d, was included to improve the energy output for large atoms [45]. H<sub>2</sub>O molecule and the various adsorption substrates were optimized individually, after which H<sub>2</sub>O was coupled on different positions of each substrate for optimization, observing the basic chemistry demand for the interactions of electro-negative and electropositive terminals of molecules. Gaussian output files were booted on *Multwfn* program [46] for topology analysis, Charge decomposition analysis (CDA), Density of State (DOS) plots, Simulating Scanning Tunneling Microscopy (STM) imaging, energy index (EI) and bond polarity index (BPI) analyses. While the intermolecular binding or adsorption energy (BE or AE) calculations, energy decomposition analysis (EDA), natural bonding orbital (NBO) analysis and thermodynamic studies were carried out on the Gaussian 09 software. The amount of energy required to disengage water molecules from the respective complexes is known as the adsorption energy [47]. The adsorption energies of water molecule on the various studied substrates were obtained through ground state energy determination of the various optimized complexes, and their corresponding fragments (H<sub>2</sub>O and quinolone or di-azanaphthalenes) on Gaussian. Calculated energies was transformed

to BE using the traditional expression for adsorption energy, as indicated in Eq. (1).

$$B.E = E_{(substrate)} + E_{(H_2O)} - E_{(complex)} \quad (1)$$

Where  $E_{(substrate)}$ ,  $E_{(H_2O)}$  and  $E_{(complex)}$  are the energies of the substrate, water molecule and complex respectively. For a fair understanding of the energy decomposition between specific fragments of the various molecular clusters, we employed the EDA method based on classical forcefield (EDA-FF). The B3LYP/631-G (d) optimized clusters were disintegrated into its corresponding fragments, which were loaded into *Multwfn* program for EDA-FF analysis. The total interaction energy ( $E_{tot}$ ), electrostatic interaction ( $E_{els}$ ), exchange repulsion ( $E_{ex}$ ) and orbital interaction ( $E_{orb}$ ) terms obtained for the substrates, H<sub>2</sub>O and corresponding complexes as defined in Eqs. (2), (3), (4), and (5), were used to explain the interactions.

$$\Delta E_{tot} = E^{complex} - \sum E^{fragment} \quad (2)$$

$$\Delta E_{tot} = \Delta E_{els} + \Delta E_{ex} + \Delta E_{orb} \quad (3)$$

$$\Delta E_{orb} = \Delta E_{SCF\_last} - \Delta E_{SCF\_1st} \quad (4)$$

$$\Delta E_{els} + \Delta E_{ex} = \Delta E_{tot} - \Delta E_{orb} \quad (5)$$

Where  $\Delta E_{SCF\_last}$  and  $\Delta E_{SCF\_1st}$  are the self-consistent field (SCF) energies for the last and first cycles respectively, of the SCF procedure as obtained [48]. In order to understand the donor-acceptor interactions of the fragments in the complexes, CDA was carried out. Intermolecular interactions in our current study are all N—H and O—H in nature, and for each case N and O atoms employ their lone pair of electrons in interacting with the unoccupied orbitals of H atom. The next transfer of electron density from fragment 1 (substrate) to 2 (H<sub>2</sub>O) is obtainable from extended CDA [49]. Topology analysis (through Atom in molecules (AIM) analysis) were carried out on *Multwfn* program, in other to understand the hydrogen bonds formed between fragments in the complexes. Hydrogen bond B.E were calculated from the electron densities ( $\rho$ ) of critical points (CPs) of the various intermolecular H-bonds, using Eq. (6), peculiar for neutral H-bond. CP properties were used to calculate Shannon aromaticity of the rings.

$$H\text{-Bond B.E} = -223.08 \times \rho(r_{BCP}) + 0.7423 \quad (6)$$

Where  $\rho$  and B.E are obtained in a.u. and kcal/mol respectively [50].

The polarity on the intermolecular bonds between the two fragments was studied by determining the bond polarity index (BPI) and energy index (EI) of the bonds. Energy index of reference and fragment atoms of the binding sites of fragments groups were obtained from *Multwfn* program. While the BPI were obtained using Eq. (7).

$$BPI = (EI_{frag1} - EI_{frag1}^{ref}) - (EI_{frag2} - EI_{frag2}^{ref}) \quad (7)$$

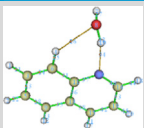
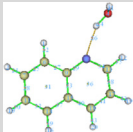
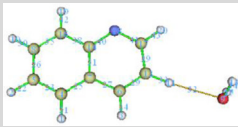
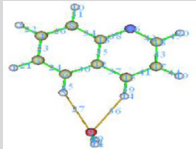
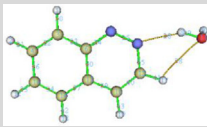
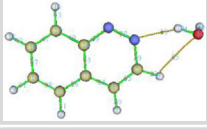
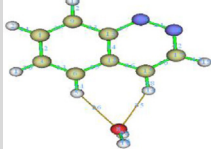
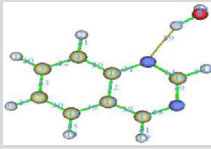
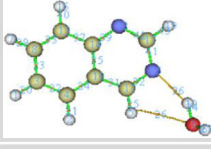
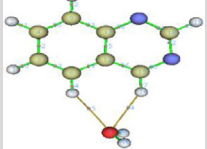
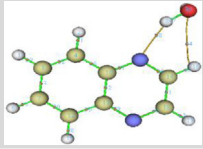
Where  $EI_{frag1}$ ,  $EI_{frag1}^{ref}$ ,  $EI_{frag2}$  and  $EI_{frag2}^{ref}$  are the energy indices for fragment 1, fragment 1 reference, fragment 2 and fragment 2 reference, respectively [51]. The thermodynamic properties; Enthalpy and Gibbs free energy of formation of the various complexes were considered in this study. This was carried out through frequency calculations on the complexes, substrate and H<sub>2</sub>O, using B3LYP/631-G(d) method.  $\epsilon_0$  (total electron energy),  $\epsilon_{ZPE}$  (zero-point energy),  $E_{tot}$  (thermal energy),  $H_{corr}$  (thermal enthalpy) and  $G_{corr}$  (thermal free energy) terms are obtained from the Gaussian outputs for H<sub>2</sub>O, complexes and corresponding substrates.

$$H_{corr} = E_{tot} + K_B T \quad (8)$$

Where  $K_B$  and  $T$  are Boltzman constant and temperature respectively,

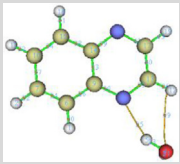
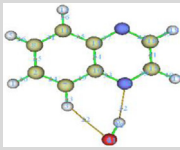
$$G_{corr} = H_{corr} - TS_{tot} \quad (9)$$

**Table 1.** Structures, compositions, position of attachment and titles of various complexes studied with DFT/3BLYP method and 631 G (d) subset.

S/N	Optimized structures	Composition/interaction position	Title
1		Quinoline + H <sub>2</sub> O (1)	QNOL1
2		Quinoline + H <sub>2</sub> O (2)	QNOL2
3		Quinoline + H <sub>2</sub> O (3)	QNOL3
4		Quinoline + H <sub>2</sub> O (4)	QNOL4
5		Cinnoline + H <sub>2</sub> O (2)	CNOL2
6		Cinnoline + H <sub>2</sub> O (3)	CNOL3
7		Cinnoline + H <sub>2</sub> O (4)	CNOL4
8		Quinazoline + H <sub>2</sub> O (2)	QNAZ2
9		Quinazoline + H <sub>2</sub> O (3)	QNAZ3
10		Quinazoline + H <sub>2</sub> O (4)	QNAZ4
11		Quinoxaline + H <sub>2</sub> O (2)	QNOX2

(continued on next page)

Table 1 (continued)

S/N	Optimized structures	Composition/interaction position	Title
12		Quinoxaline + H <sub>2</sub> O (3)	QNOX3
13		Quinoxaline + H <sub>2</sub> O (4)	QNOX4

N/B → Binding site position numbers starts with the first N atom on ring 1, and proceeds in a clockwise direction.

Where  $S_{tot}$  is the total entropy of the system, which is defined in Eq. (10) below.

$$S_{tot} = S_t + S_r + S_v + S_e \quad (10)$$

Where  $S_b$ ,  $S_p$ ,  $S_v$  and  $S_e$  are the translational, rotational, vibrational and electronic entropy contributions.

The enthalpies and Gibbs free energies of formation of the various titled clusters were obtained using Eqs. (11), (12), and (13). Where calculations were performed at STP (T = 298K; P = 1 atm)

$$\Delta_f H^0 (298K) = [\Sigma \Delta_f H^0_{products}(298K) - \Sigma \Delta_f H^0_{reactants}(298K)] \times 627.5095 \quad (11)$$

The constant 627.5095 is a factor to covert energy from Hartree to kcal/mol. But from the electronic and thermal energy, which are obtainable from the Gaussian 09 calculations, one can easily determine the  $\Delta_f H^0$  for the clusters.

$$\Delta_f H^0 (298K) = [\Sigma(\epsilon_0 + H_{corr})_{products} - \Sigma(\epsilon_0 + H_{corr})_{reactants}] \times 627.5095 \quad (12)$$

$$\Delta_f G^0 (298K) = [\Sigma(\epsilon_0 + G_{corr})_{products} - \Sigma(\epsilon_0 + G_{corr})_{reactants}] \times 627.5095 \quad (13)$$

Eqs. (8), (9), (10), (11), (12), and (13) was adopted from the reports from Ochterski in 2000 [52,53].

Natural bonding orbital (NBO) analysis was carried out on Gaussian 09, in order to study the orbital interactions leading to complex stabilization. Interaction with significant energy contributions are considered and interpreted. The electrostatic potential (ESP) and STM plots was done on Gaussview software and *Multwfn* program respectively, using total electron distribution.

### 3. Results and discussion

#### 3.1. Adsorption energy studies

Adsorption energy or binding energy of a complex is defined as the amount of energy required to dissociate the complex into its basic components, this is equal the magnitude of energy required to bind the components [54]. The intermolecular binding energy was analyzed to expose details of grip strength, bond strength and relative stability of the complexes. Positive values of adsorption energy imply that there is desorption, while negative values are indicative of adsorption. The adsorption energies as reported in Table 2., were calculated using Eq. (1), from the individual energy values of the clusters and components, obtained from single point energy calculations of the DFT/B3LYP optimized structures.

From the adsorption energies in Table 2., where negative BE values was obtained for all studied complexes, one can infer that there was an overall adsorption of H<sub>2</sub>O molecules on the various substrates at all binding sites. Relatively, the diazanaphthalene-H<sub>2</sub>O complexes are more chemically held together than the various quinoline-H<sub>2</sub>O complexes, owing to the less negative values of BE for quinoline based complexes. Highest BE value of -3.99 eV is recorded for CNOL4, which implies that water molecule is strongly adsorbed at position 4 of cinnoline. This is predicted to be due to the formation of a di-hydrogen bonding between O atom of water molecule and two H atoms of cinnoline, as can be visualized on the CNOL4 structure in Table 1. Best overall binding is noticeable for quinoxaline + H<sub>2</sub>O (QNOX) clusters, with B.E < -3.90 eV for all studied binding sites, as can be visualized in Figure 1.

Table 2. Adsorption energies, energy decomposition terms from energies of clusters, substrates and H<sub>2</sub>O of various complexes studied with DFT/3BLYP method and 631 G (d) basis.

Clusters	Adsorption energy (EV)	Total energy term $\Delta E$ (TOT) KCAL/MOL	Polarization term $\Delta E_{(ORB)}$ KCAL/MOL	Steric term $\Delta E_{(EL,S)} + \Delta E_{(EX)}$ KCAL/MOL
QNOL1	-3.66	-9.73	-159.89	<b>150.16</b>
QNOL2	-3.71	-8.53	-160.39	<b>151.86</b>
QNOL3	-3.95	-2.95	-162.02	<b>159.07</b>
QNOL4	-3.91	-3.77	-161.14	<b>157.38</b>
CNOL2	-3.81	-8.66	-148.47	<b>139.81</b>
CNOL3	-3.81	-8.72	-148.47	<b>139.74</b>
CNOL4	-3.99	-4.45	-145.96	<b>141.50</b>
QNAZ2	-3.85	-7.66	-145.08	<b>137.42</b>
QNAZ3	-3.83	-8.09	-145.52	<b>137.42</b>
QNAZ4	-3.98	-4.52	-144.76	<b>140.25</b>
QNOX2	-3.98	-7.66	-143.20	<b>135.54</b>
QNOX3	-3.98	-7.66	-143.26	<b>135.60</b>
QNOX4	-3.93	-9.04	-143.20	<b>134.16</b>

The figures in bold are significant in the discussion, so they were segregated for easy visualizing.

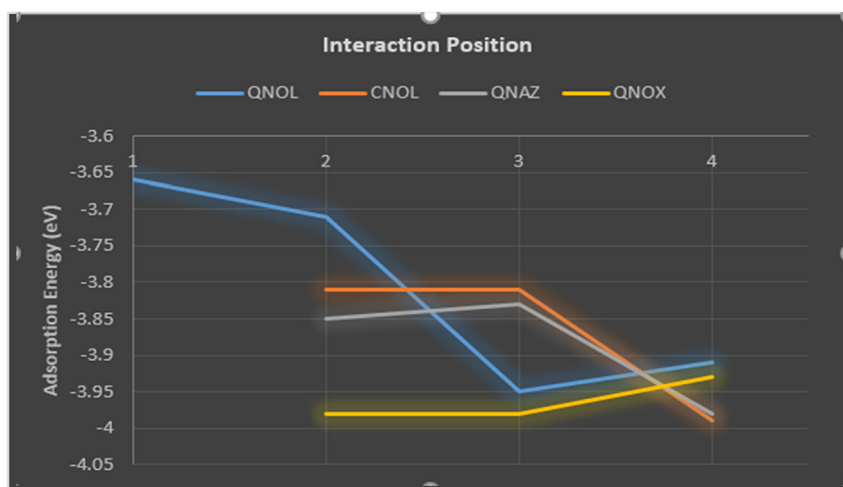


**Figure 1.** Plots of Adsorption energies for the various interactions positions in QNOL, CNOL, QNAZ and QNOX studied with DFT/B3LYP method and 631-G (d) basis set.

### 3.2. Energy decomposition studies

EDA was carried out in order to understand the extent of interactions between adsorbed H<sub>2</sub>O molecules and the various substrates. The total interaction energy term ( $\Delta E_{\text{(tot)}}$ ) explains the amount of energy existing between two fragments, with which one can understand the linkage chemistry [55, 56]. Orbital interaction energy term ( $\Delta E_{\text{(orb)}}$ ), also known as the polarization term is used to determine the level of orbital interactions between the molecular orbitals (MOs) of the fragment, which stabilizes the adduct. Also, the sum of the electrostatic and exchange-repulsion energy terms ( $\Delta E_{\text{(els)}} + \Delta E_{\text{(ex)}}$ ) defines the level of steric hindrance around the interaction sites of clusters. This hindrance is as a result of the arrangement of the vicinal groups ([N or C] and their substituents) to the binding sites. The  $\Delta E_{\text{(tot)}}$ ,  $\Delta E_{\text{(orb)}}$ , and  $\Delta E_{\text{(els)}} + \Delta E_{\text{(ex)}}$  for the various complexes at B3LYP/631-G (d) are reported in Table 2. From the  $\Delta E_{\text{(tot)}}$  values in Kcal/mol as reported in Table 2., it is evident that QNOL1 (-9.73), CNOL2 (-8.66), CNOL3 (-8.72), QNAZ3 (-8.09), QNOX2 (-7.66), QNOX3 (-7.66) and QNOX4 (-9.04), where dual interaction bonds of N—H and O—H are confirmed to exist between H<sub>2</sub>O and

substrate, exhibited good interactions, hence are classified to be relatively stable clusters. A relatively weak dual interaction where the oxygen atom of H<sub>2</sub>O form intermolecular bonds with two hydrogens of the substrate is evident in QNAZ4 (-4.52). This weakness in dual bond is expected because it is a projection from the oxygen of H<sub>2</sub>O to two hydrogen atoms of the substrate, exhibiting a lower electron density. Very weak interaction energies were obtained for QNOL3, QNOL4, CNOL4 and QNAZ4. Overall, the high  $\Delta E_{\text{(tot)}}$  values of quinoxaline-H<sub>2</sub>O clusters indicates that the complexes are more stable. Better stabilization is predicted CNOL2, CNOL3 and QNAZ3 in their various groups, owing to their higher  $\Delta E_{\text{(orb)}}$  values, although the differences recorded for the different clusters aren't obvious. High  $\Delta E_{\text{(els)}} + \Delta E_{\text{(ex)}}$  are observed for CNOL4, QNAZ4 and QNOX3 clusters, this is interpreted to represent a high steric hindrance around their binding sites.

### 3.3. Density of state (DOS) analysis

The partial, total and overlap population density of states (PDOS, TDOS and OPDOS) were plotted for all cluster interactions to understand

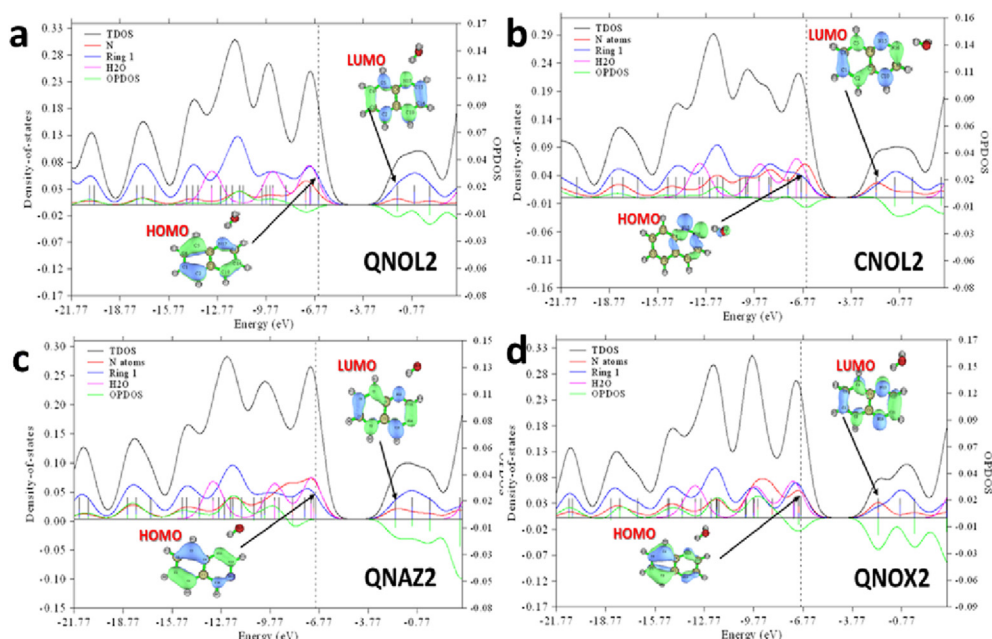


**Figure 2.** PDOS, TDOS and OPDOS Plots for (a) QNOL2, (b) CNOL2, (c) QNAZ2 and (d) QNOX2 studied with DFT/B3LYP method and 631-G (d) basis set.



the orbital compositions of the different MOs in the complexes [57]. The PDOS, TDOS and OPDOS plots for QNOL2, CNOL2, QNAZ2 and QNOX2 (representative of their various groups) are presented in Figure 2 for a comparative study of the various substrates. The complexes are split into fragments of interest, so as to visualize the contributions of the various groups in the studied complex. The Nitrogen atoms contribution is represented with orange curve, H<sub>2</sub>O with pink, and the heterocyclic ring with blue curve.

One can visualize from Figure 2., that for QNOL2, CNOL2, QNAZ2 and QNOX3, ring 1 (blue) and N atoms (orange) correspond to the PDOS curve (green), hence the heterocyclic ring and nitrogen groups contribute largely to the stability of the clusters. Negative value for PDOS is indicative of antibonding interaction at the corresponding MO. This implies that CNOL2 and QNOX2 exhibits antibonding characters at their HOMO levels, which arises from the inadequate overlap of MOs. All clusters discussed experienced antibonding properties at LUMO, as visualized from the polarity of PDOS curve at this point. The effect of the heterocyclic ring is maximum between -12.77— -9.77 eV for all studied complexes, this implies that the aromatic ring has its highest contribution to the MOs within this range. It is evident that H<sub>2</sub>O molecular orbital contribution is highest at HOMO for all complexes, as can be visualized from its high curve at HOMO levels.

### 3.4. Scanning tunneling microscopy (STM)

STM technique is employed in imaging chemical systems at their atomic level, it is directly related with the electronic composition of the chemical system. STM plot is a special tool in understanding the tunneling current (*I*) distribution around molecules. Tunneling current is directly proportional to local density of state (LDOS) [58]. In visualizing STM diagrams, the bright white coloration indicates regions with high LDOS, hence strong tunneling current. In this study, the STM plots for QNOL2, CNOL2, QNAZ2 and QNOX2 (representative of their various groups) are presented in Figure 3.

A high tunneling current is observable around the C atoms of Ring 2 of QNOL2, QNAZ2 and QNOX2 (Figure 3), as can be inferred from the

bright white coloration around these regions. Mild distribution of *I* around C–N bonds in the various complexes is visible, except for CNOL2, where a bright white surface is concentrated on the N atoms. It is evident that tunneling current (*I*), hence electron density and LDOS is highly concentrated on the N heteroatoms of CNOL2 complex. Much similarity is confirmed for the electronic distribution of *I* around complex molecules in QNOL, QNAZ and QNOX, but CNOL.

### 3.5. Charge decomposition studies

Charge decomposition analysis (CDA) and extended CDA are carried out to understand the mechanism of charge transfer between H<sub>2</sub>O fragment and substrates in the various studied complexes to obtain charge equilibrium [59]. The studied interactions in the project are basically N–H and O–H in nature, where N and O uses their lone pair of electrons to interact with the unoccupied orbital of H. Extended CDA is used to determine the net transfer of electrons from substrate to H<sub>2</sub>O in the complex [49]. ECDA excludes the electronic contributions from polarization effect (PL) making it a better approach than the general ECDA. The ECDA results for all studied clusters are presented in Table 3. The substrates are defined as fragment 1, and H<sub>2</sub>O moiety as fragment 2 for the various ECDA determinations (Figure 4).

From Table 3., the net amount of electrons transferred to fragment 2 is deduced by subtracting the electron density back-donated from fragment 2 to 1 (CT 2→1) from the amount donated from fragment 1 to 2 (CT 1→2). Overall, there is net electron transfer from fragment 2 to 1 in QNOL3, QNOL4, CNOL4 and QNAZ4, as depicted in the negative values of net electron obtained. This is because the O atom in H<sub>2</sub>O was used in binding for these complexes. The other complexes exhibited a net electron transfer from fragment 1 to 2, which is traced to the N→H binding that took place in many clusters studied. It is worthy to note that the QNOL2 (0.0369) exhibit the highest net electron transfer from substrate to H<sub>2</sub>O. Also, appreciable  $\pi$ -back donation properties are predicted for QNOL3, QNOL4, CNOL4 and QNAZ4, owing to their high net electron transfer from fragment 2→1, which is as a result of depleted overlap region between the two fragments in such systems [59]. This observation

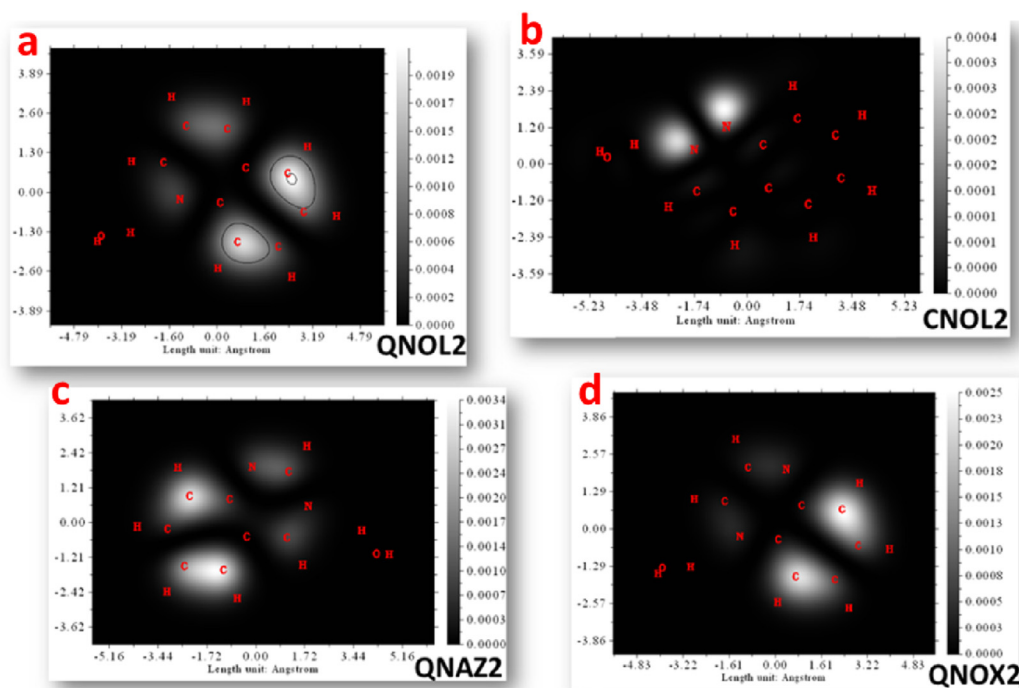
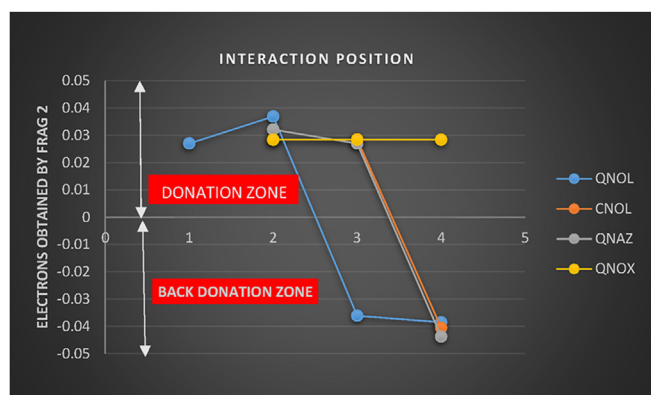


Figure 3. STM images of (a) QNOL2, (b) CNOL2, (c) QNAZ2 and (d) QNOX2 studied with DFT/B3LYP method and 631-G (d) basis set.

**Table 3.** Net electron transfer between fragments from ECDA for clusters studied with DFT/3BLYP method and 631 G (d) basis.

Cluster	Net Electron Transfer Frag 1→2	Net Electron Transfer Frag 2→1	Net Electrons Obtained by Frag 2
QNOL1	0.0762	0.0492	0.0270
QNOL2	0.0677	0.0308	<b>0.0369</b>
QNOL3	0.0023	<b>0.0384</b>	-0.0361
QNOL4	0.0030	<b>0.0414</b>	-0.0385
CNOL2	0.0607	0.0323	0.0284
CNOL3	0.0608	0.0323	0.0285
CNOL4	0.0031	<b>0.0437</b>	-0.0405
QNAZ2	0.0626	0.0305	0.0321
QNAZ3	0.0562	0.0292	0.0270
QNAZ4	0.0033	<b>0.0470</b>	-0.0437
QNOX2	0.0612	0.0328	0.0284
QNOX3	0.0635	0.0351	0.0284
QNOX4	0.0601	0.0317	0.0284

The figures in bold are significant in the discussion, so they were segregated for easy visualizing.



**Figure 4.** Plots of Electron Obtained by Fragment 2 ( $H_2O$ ) from CDA for the various interactions positions in QNOL, CNOL, QNAZ and QNOX studied with DFT/B3LYP method and 631-G (d) basis set.

can be visualized clearly in Figure 5. Orbital interaction diagrams (Figure 5.) were plotted for QNOL2, CNOL2, QNAZ2 and QNOX2, in order to visualize the mixing of fragments orbitals as the complexes are obtained.

The fragment orbitals of fragment 1 (substrate) are aligned to the left, fragment 2 ( $H_2O$ ) to the right and cluster orbitals at the middle. Linking (red lines) connects fragment orbitals (FOS) with electron composition higher than 10% [59, 60]. Substrate FOs 16, 17 and 18 are linked with complex orbitals (COs) 18, 19 and 20 respectively in QNOL2, CNOL2, QNAZ2 and QNOX2, which implies that FOs 16, 17 and 18 are unperturbed during the formation of the respective complexes. They are  $\pi$  in nature, hence cannot partake in  $\sigma$ -type donor-acceptor interactions between complex fragments. The interactions of FOs of  $H_2O$  with the COs as shown in Figure 5., are equivalent in QNAZ2 and QNOX2, were FOs 3 and 4 of  $H_2O$  are linked with COs 33 and 35 respectively.

### 3.6. Electrostatic potential (ESP) studies

The electrostatic potential (ESP) images were plotted in order to visualize the electron density distribution around the atoms in the complexes. The ESP surface plots are colored from red through green to blue. Red regions represent areas with high presence of electrons, which are characterized with negative values for isosurfaces, while blue depicts deficiency in electron density (positive isosurface values are recorded for such surfaces) [61]. Isosurface plots for all studied clusters are presented

in Figure 6. From the isosurfaces in Figure 6 it is visible that high electron density is located around the N and O atoms, this corresponds to their electron pulling capacity as highly electronegative atoms. An appreciable amount of electrons is visible around the aromatic ring core for all studied clusters, this is inferred from the light green to dark red colorations around the rings. Hydrogen atoms are surrounded by deep blue colorations, which is indicative of deficiency in electron density, which results from the highly distorted bonding electron distribution in hydrogen to electronegative groups. This is evident for H on aromatic rings and on oxygen, the blue surfaces represent regions where electrons are depleted. Areas around the oxygen of  $H_2O$  fragment exhibited the highest isosurface values in all studied clusters.

### 3.7. Topology studies

The individual hydrogen bonding systems at the various binding sites are studied using atoms in molecule (AIM) basins approach [62]. All properties measured are dependent on the critical point (CP), which is considered as a point of reference in topology studies. The CP is a point between two neighboring atoms, which defines a bond or interaction found along the connection axis, it is located along the path of an existing or non-existing bond [62]. It was observed that during adsorption of  $H_2O$  on the various studied substrates, one or two Hydrogen bonds are formed between the fragments. In each case, distinct H-bonds are treated in order to fully understand their individual contributions to the stability of the clusters obtained. Hydrogen bond length, electron densities and binding energies are calculated for every hydrogen bond CP identified, these are reported in Table 4. In extension, the shannon aromaticity (SA) of the rings of studied complexes were measured, adopting the reports of Noorzadeh and Shakerzadeh in 2010 [63,64], the results are reported in Table 5., in the supporting information. Shannon aromaticity is relative; a reason it was employed in our study. From the figures reported on Table 5., QNAZ2 exhibited the highest aromaticity (SA = 0.0745), representing a good stabilization around the ring structure of the substrate fragment. It is observed that QNOX4 (with SA = 0.00192) is the most aromatic in its group, this supports the claim that position 4 of QNOX is the most suitable for  $H_2O$  adsorption. Relatively low aromaticity is shown by all QNOL complexes, but QNOL (with SA = 0.00198), hence  $H_2O$  adsorption on position 1 stabilized the aromatic rings of QNOL.

#### 3.7.1. Hydrogen bond length

From the measured bond length in Angstrom ( $\text{\AA}$ ) reported in Table 4., it is evident that N—H bonds are shorter than O—H bonds in

the various studied clusters. CNOL1 and CNOL2 exhibited the shortest N—H bond in this study, this implies that if we consider all H<sub>2</sub>O fragments binding on the substrates, CNOL1 and CNOL2 are more compacted at N sites. O—H bonds are perceived to naturally be longer than other counterparts [65].

### 3.7.2. Hydrogen bond binding energy

The H-bond B.E were calculated from the electron density values determined for various CPs, employing Eq. (6). They are presented in Table 4., as obtained in Kcal/mol. It is conspicuous that O—H interactions are stronger than N—H, inferable from their relative binding energies, despite the supposed contradictions from the bond length values. Hence, bond strength is not only dependent on the length but also on the electronic composition of the bonding atoms. With a closer at Table 4., one can observe a high deal of stabilizing binding energies for the O—H interactions in QNOL4 (-181.13 kcal/mol), CNOL2 (-200.12 kcal/mol), CNOL3 (-199.76 kcal/mol), CNOL4 (-189.46 kcal/mol), QNAZ4 (-176.65 kcal/mol), QNOX2 (-193.09 kcal/mol) and QNOX3 (-192.72 kcal/mol). These binding energies are crucial components of the overall cluster stabilization energies (a reason for the high cluster B.E for CNOL4 and QNAZ4 as observed from the adsorption energy study).

### 3.8. Energy index (EI) and bond polarity index (BPI)

Energy index is a useful tool in the description of the nature of electron sharing between atoms in a covalent system. Traditionally, electrons are shared equally between bonding atoms in nonpolar covalent bond, while polar covalent bond involves a distorted electron distribution density. On the other hand, bond polarity index (BPI) explains the polarity of a bond [66]. BPI was analyzed to ascertain hydrogen bond polarity between fragments in the various studied clusters. To calculate the BPI for N—H and O—H bonds in substrate + H<sub>2</sub>O complexes, the reference EI values of N and H atoms for each substrate was initially calculated, and O and H atoms in H<sub>2</sub>O molecule. The BPI were determine by invoking Eq. (7)., and the results are presented in Table 6. The EI of the various references and fragments in clusters are reported in Table 7.

As can be seen from the BPI values for the various inter-fragment bond in Table 6., highly negative BPI are derived for N—H intermolecular linkages, which implies that they are more polar, so can be relatively classified as polar covalent bonds. This is due to distortion in the electron distribution along the binding part in such clusters. QNOL1, QNOL2, CNOL2, CNOL3, QNAZ3 and QNOX4 with bond polarity indices; -0.11, -0.014, -0.069, -0.074 and -0.09 respectively are appreciably polar at binding sites. Hence, they are predicted to be more soluble in aqueous

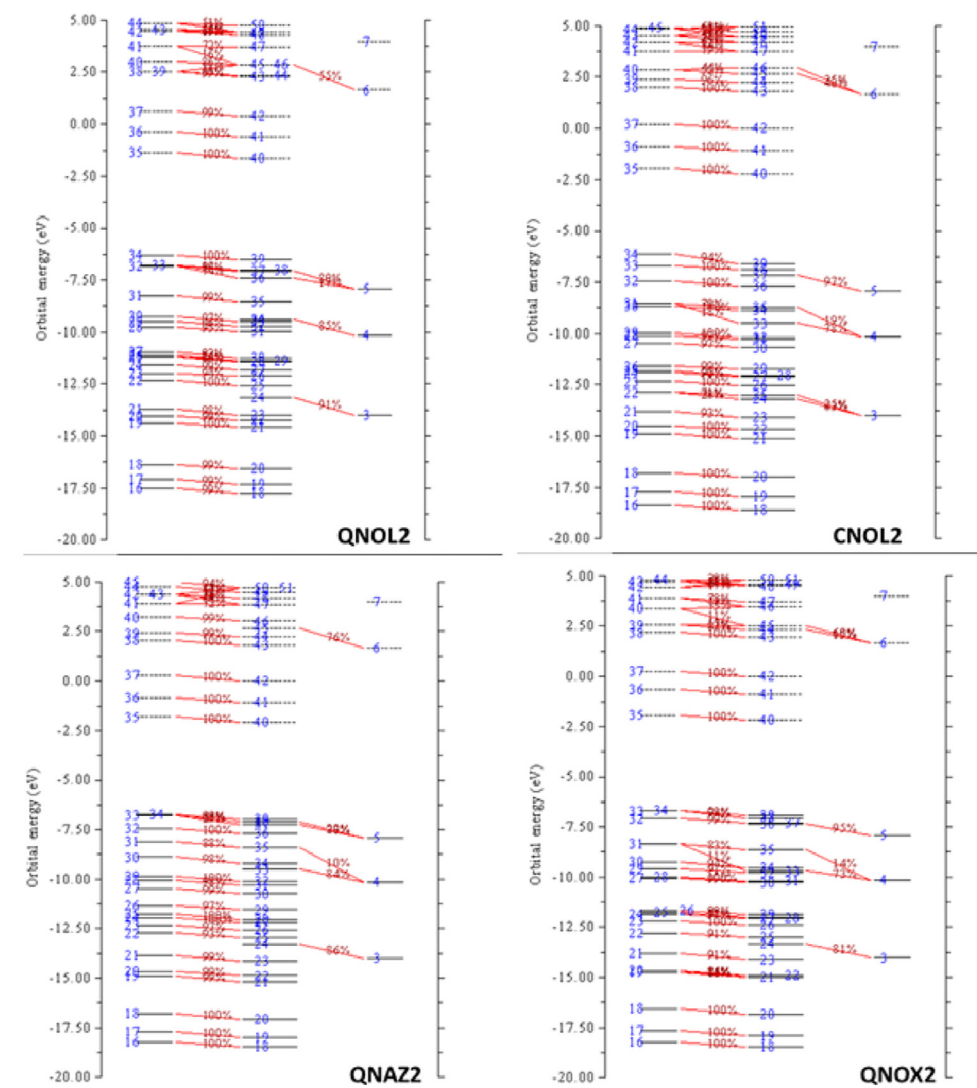


**Figure 5.** Orbital interaction diagrams from CDA for the various interactions positions in QNOL, CNOL, QNAZ and QNOX studied with DFT/B3LYP method and 631-G (d) basis set.



systems. O—H linkages are less polar to N—H bonds in our studied clusters. This is due to the extended system (C—H—O—H), where electrons are more evenly distributed than C=N—H—O for N adsorption sites.

### 3.9. Thermodynamics considerations

Thermodynamics studies the relationship between work and heat energy, as both changes on the course of a chemical reaction [67]. In order to understand the feasibility of the formations and stabilities of the studied clusters, we considered the enthalpies ( $\Delta H$ ) and Gibbs free energies ( $\Delta G$ ) of formation. The Gibbs free energy; a function of enthalpy change ( $\Delta H$ ), entropy change ( $\Delta S$ ), and temperature, explains the spontaneity of a chemical reactions [52]. The total electron energy ( $\epsilon_0$ ), zero-point energy ( $\epsilon_{zpe}$ ), thermal energy ( $E_{tot}$ ), total entropy ( $S_{tot}$ ) thermal enthalpy ( $H_{corr}$ ), and thermal free energy ( $G_{corr}$ ) terms required from Gaussian 09 output, in the calculations of  $\Delta H_f$  and  $\Delta G_f$  of the various complexes were calculated. All thermodynamic calculations are done at

298.15K and 1atm, considering one mole of complex, by applying Eqs. (8), (9), (10), (11), (12), and (13). The thermodynamics parameters of all studied fragments were calculated with DFT/B3LYP method at 631-G (d) basis, the  $\Delta H_f$  of water at STP is calculated to be -76.384 eV at this level.

Positive  $\Delta H_f$  values are obtained for all studied clusters (Table 8), which is interpreted as endothermic, this implies that heat is absorbed from the surrounding during their formation process. It is notable that QNOL, CNOL, QNAZ and QNOX interacts with H<sub>2</sub>O molecules by absorbing a deal of energy from the surroundings, hence a cooling effect is felt when they are solvated. The change in enthalpy for the formation of QNOX4 (+59.17 kcal/mol) is the least for the studied binding sites in QNOX, hence binding at position 4 of QNOX absorbs the least amount of energy. CNOL4 formation is accompanied with the highest energy absorption, this is explained by its high  $\Delta H_f$  value (62.85 kcal/mol).

The calculated  $\Delta G_f$  values for all complexes at 298.15K and 1atm, as can be seen in Table 8., are positive, this is an implication that the formation process of all the studied complexes are nonspontaneous in

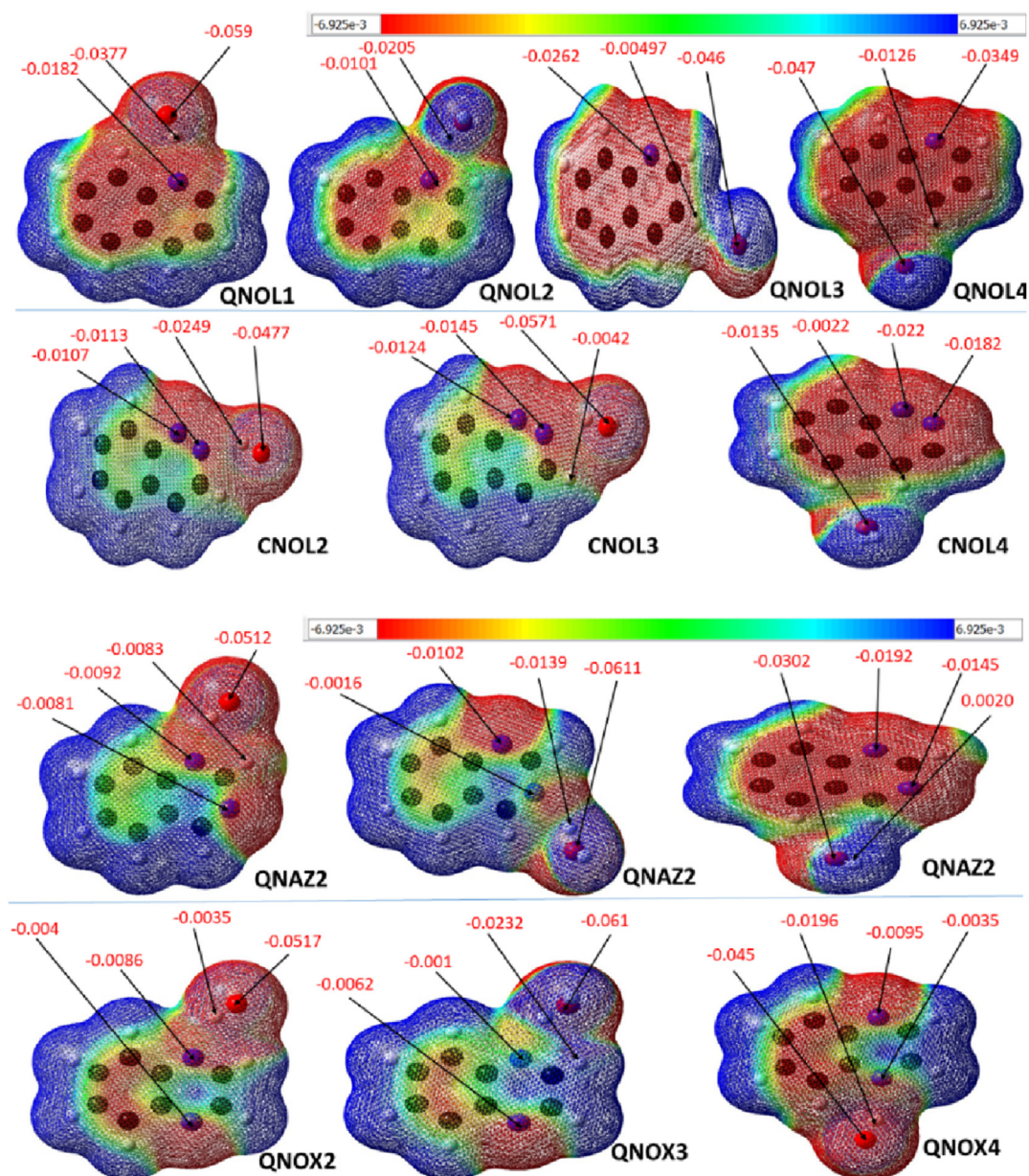


Figure 6. ESP Isosurface plots for all Clusters studied with DFT/B3LYP method and 631-G (d) basis set.

**Table 4.** Measured H-bond lengths, H-bond electron densities, and H-bond binding energy from AIMs analysis of all clusters studied with DFT/B3LYP method and 631-G (d) basis set.

Clusters	Identified H-bonds	CPS number	Bond length (Å)	Density (A.U)	H-Bond B.E (KCAL/MOL)
QNOL1	O18 – H13	26	2.42	0.12	-26.23
	N16 – H19	34	<b>1.98</b>	0.30	-65.36
QNOL2	N17 – H20	26	<b>1.98</b>	0.29	-64.02
QNOL3	O18 – H7	32	2.39	0.13	-28.15
QNOL4	O18 – H8	27	2.49	0.82	<b>-181.13</b>
	O18 – H6	36	2.55	0.10	-21.70
CNOL2	N16 – H19	28	2.01	0.27	-60.43
	O17 – H14	38	2.58	0.90	<b>-200.12</b>
CNOL3	O17 – H14	25	2.58	0.90	<b>-199.76</b>
	N16 – H19	35	2.00	0.27	-60.58
CNOL4	O17 – H7	26	2.44	0.85	<b>-189.46</b>
	O17 – H9	35	2.54	0.11	-23.48
QNAZ2	N15 – H19	29	2.01	0.27	-60.02
QNAZ3	O17 – H16	26	2.64	0.80	-178.61
	N14 – H19	36	2.06	0.24	-53.51
QNAZ4	O17 – H7	25	2.50	0.80	<b>-176.65</b>
	O17 – H9	34	2.57	0.11	-22.79
QNOX2	O14 – H18	28	2.61	0.27	-58.82
	N13 – H16	34	2.01	0.87	<b>-193.09</b>
QNOX3	N16 – H18	25	2.02	0.27	-58.71
	O17 – H14	29	2.61	0.87	<b>-192.76</b>
QNOX4	O14 – H8	22	2.41	0.12	-26.63
	N19 – H16	32	2.01	0.28	-60.74

The figures in bold are significant in the discussion, so they were segregated for easy visualizing.

nature. Hence a given amount of energy is required to propel the various reactions leading to our studied clusters. It is evident that  $\Delta S$  is negative, due to the positive values obtained for  $\Delta G_f$  and  $\Delta H_f$  (eqn 9) respectively. In comparison, the formation of QNOX4 is an easier process than of other QNOX complexes, because of its lower  $\Delta G_f$  value (+67.89 kcal/mol) in the group. CNOL4 is more difficult to obtained, comparing the  $\Delta G_f$  value (+68.33), which is the highest for CNOL complexes. Hence, binding of H<sub>2</sub>O molecule are position 4 of CNOL is more difficult, although, it gives the most stable complex (as discovered from B.E studies). It is visible from  $\Delta G_f$  values in Table 8., that QNOL + H<sub>2</sub>O are the easiest to obtain, they exhibited a comparably low  $\Delta G_f$  values.

**Table 5.** Measured Shannon aromaticity indices from AIMs analysis of all clusters studied with DFT/B3LYP method and 631-G (d) basis set.

Clusters	Shannon aromaticity
QNOL1	0.00198
QNOL2	0.00138
QNOL3	0.00153
QNOL4	0.00154
CNOL2	0.00422
CNOL3	0.00421
CNOL4	0.00411
QNAZ2	0.07454
QNAZ3	0.00216
QNAZ4	0.00221
QNOX2	0.00188
QNOX3	0.00188
QNOX4	0.00192

N/B; Shannon aromaticity is relative.

### 3.10. Natural bonding orbitals (NBO) analysis

The stabilization energies (second perturbation energies) of the interacting NBOs of the studied complexes with significant energies are considered in this research [68, 69]. It was inferred from the Shannon aromaticity studies that the presence on N atoms in the aromatic ring backbone improved the overall aromaticity of the studied complexes, where QNOL + H<sub>2</sub>O clusters exhibited lower aromaticity, hence less stable rings. Very important interactions are expected from the bonding orbitals of N atoms with other orbitals to attain more stability for complexes. The second perturbation energies of the natural bonding orbitals of the studied

**Table 6.** Calculated BPI values for various intermolecular bonds of all clusters studied with DFT/B3LYP method and 631-G (d) basis set.

Clusters	Bond type rEF1—rEF2	BPI
QNOL1	N—H	<b>-0.110</b>
QNOL2	H—O	-0.014
QNOL3	H—O	0.055
QNOL4	H—O	0.065
CNOL2	N—H	<b>-0.069</b>
CNOL3	H—O	-0.011
CNOL4	H—O	0.072
QNAZ2	H—O	0.076
QNAZ3	N—H	<b>-0.074</b>
QNAZ4	H—O	0.067
QNOX2	H—O	-0.0003
QNOX3	H—O	-0.0003
QNOX4	N—H	<b>-0.090</b>

The figures in bold are significant in the discussion, so they were segregated for easy visualizing.

**Table 7.** Calculated fragment and reference EI and BPI values for various intermolecular bonds of all clusters studied with DFT/B3LYP method and 631-G (d) basis set.

Clusters	Bond type REF1-REF2	EI of binding site on REF1	EI of binding site on REF2	EI of binding sites on FRAG1	EI of binding site on FRAG2	BPI
QNOL1	N-H	-0.5	-0.605	-0.542	-0.537043	-0.11012
QNOL2	H-O	-0.48	-0.534	-0.465	-0.500291	-0.0135
QNOL3	H-O	-0.49	-0.534	-0.461	-0.554698	0.054805
QNOL4	H-O	-0.5	-0.534	-0.458	-0.560775	0.065366
CNOL2	N-H	-0.53	-0.605	-0.54	-0.542198	-0.06919
CNOL3	H-O	-0.5	-0.534	-0.477	-0.50337	-0.01098
CNOL4	H-O	-0.51	-0.534	-0.471	-0.567065	0.072141
QNAZ2	H-O	-0.57	-0.534	-0.469	-0.505136	0.076012
QNAZ3	N-H	-0.52	-0.605	-0.545	-0.55447	-0.07363
QNAZ4	H-O	-0.5	-0.534	-0.466	-0.562777	0.067252
QNOX2	H-O	-0.5	-0.534	-0.478	-0.51091	-0.00026
QNOX3	H-O	-0.5	-0.534	-0.478	-0.510929	-0.00026
QNOX4	N-H	-0.53	-0.605	-0.56	-0.54952	-0.09003

N/B; Fragment 1 = Substrate (QNOL, CNOL, QNAZ and QNOX).

Fragment 2 = H<sub>2</sub>O.

EI of Ref1 = EI of N or H atoms in substrate as applicable, depended on binding site.

EI of Ref2 = EI of O or H atoms in H<sub>2</sub>O as applicable.

**Table 8.** Change in enthalpies ( $\Delta H_f$ ) and Gibbs free energies ( $\Delta G_f$ ) of formation from Gaussian 09 calculations at 298.15K and 1atm for all clusters studied with DFT/B3LYP method and 631-G (d) basis set.

Clusters	$\Delta H_f$ (KCAL/MOL)	$\Delta G_f$ (KCAL/MOL)
QNOL1	<b>55.81</b>	64.60
QNOL2	56.99	65.38
QNOL3	61.90	66.75
QNOL4	60.61	66.99
CNOL2	59.09	67.55
CNOL3	59.09	67.55
CNOL4	<b>62.85</b>	<b>68.33</b>
QNAZ2	60.31	68.61
QNAZ3	59.84	68.21
QNAZ4	63.01	69.35
QNOX2	60.31	68.65
QNOX3	60.31	68.64
QNOX4	<b>59.17</b>	<b>67.89</b>

The figures in bold are significant in the discussion, so they were segregated for easy visualizing.

complexes are presented in Table 9  $n \rightarrow \sigma^*$  and  $n \rightarrow \pi^*$  donor acceptor resonance interactions of heteroatoms leads to stability. This type of interaction is evident in for all studied complexes; e.g.  $nC3 \rightarrow \pi^*C1-C2$  (49.96 kcal/mol)/ $\pi^*C10-C13$  (54.43 kcal/mol)  $nN15 \rightarrow \sigma^*C3-C4$  (10.34 kcal/mol) in CNOL2 and  $nC4 \rightarrow \pi^*C5-C6$  (48.69 kcal/mol)/ $\pi^*N13-C17$  (60.81 kcal/mol) in QNOX2,  $nC4 \rightarrow \pi^*C5-C6$  (49.44 kcal/mol)/ $\pi^*C11-N15$  (59.18 kcal/mol) in QNOX3 and  $nC3 \rightarrow \pi^*C1-C2$  (Kcal/mol)/ $\pi^*C11-N19$  (Kcal/mol) in QNOX4 are good stabilizing interactions with significant energies of stabilization. Other very important second order perturbations are the  $\pi \rightarrow n^*$  and  $\pi \rightarrow \pi^*$  types, they correspond to the hyper-conjugative interactions of the aromatic rings. Our utmost interest is in those involving N atoms of the ring;  $\pi N15-N16 \rightarrow n^*C4$  (28.99 kcal/mol)/ $\pi^*C10-C13$  (16.25 kcal/mol) in CNOL2,  $\pi N15-N16 \rightarrow n^*C4$  (29.00 kcal/mol)/ $\pi^*C10-C13$  (16.26 kcal/mol) in CNOL3,  $\pi N15-N16 \rightarrow \pi^*C3-C4$  (15.18 kcal/mol)/ $\pi^*C10-C13$  (16.21 kcal/mol) in CNOL4,  $\pi C13-N15 \rightarrow n^*C4$  (43.16 kcal/mol)/ $\pi^*C10-N16$  (8.97 kcal/mol) in QNAZ2,  $\pi N11-C12 \rightarrow n^*C4$  (43.53 kcal/mol)/ $\pi^*N14-C15$  (Kcal/mol) in QNAZ3,  $\pi N13-C17 \rightarrow n^*C4$  (39.07 kcal/mol)/ $\pi^*C11-N19$  (14.82 kcal/mol) in QNOX2 and  $\pi N13-C17 \rightarrow n^*C4$  (39.43 kcal/mol)/ $\pi^*C11-N19$

(16.73 kcal/mol) in QNOX4 are necessary interactions which contribute to the stabilization of the studied complexes. No orbital interaction with significant stabilization energy was observed involving H<sub>2</sub>O fragment orbitals nor fragment bonding orbitals, hence the inter-fragment interactions are generally weak. This claim agrees with the thermodynamic results of the studied complexes; All formation processes are endothermic (requires high deal of energy to proceed) and nonspontaneous (due to large  $\Delta G$  values).

#### 4. Conclusion

The inter-fragment chemistry and stability studies of complexes of quinoline, cinnoline, quinazoline and quinoxaline with H<sub>2</sub>O was achieved in this work. We discovered that H<sub>2</sub>O molecules are adsorbed on the various studied binding sites of substrates, although no much interactions are recorded between the fragments. From thermodynamic studies, we observed that the formation of the studied complexes at STP are significantly endothermic and nonspontaneous, with the complex of cinnoline with H<sub>2</sub>O at position 4 being more stable. Generally, the formation of quinoxaline + H<sub>2</sub>O complexes are more easily obtainable and are also fairly stable. Appreciable tunneling current ( $I$ ) is concentrated on the N atoms of CNOL, as revealed by visualized STM images, while much similarities exist for QNOL, QNAZ and QNOX, where  $I$  are distributed about the aromatic C atoms. We also observed from the visualized ESP diagrams of the studied complexes that electron densities are concentrated around N and O atoms of the complexes, implying that they are relatively more electronegative than other groups in the clusters. The N-H inter-fragment linkages were found to be highly polar covalent in nature from bond polarity index studies, while electronic distribution around O-H inter-fragment bonds are very even, making them less polar. From CDA results, a net charge transfers from fragment 1 (substrate) to fragment 2 (H<sub>2</sub>O) (CT 1 $\rightarrow$ 2) was revealed for most complexes, except QNAZ4, CNOL4, QNOL4 and QNOL2, where CT 2 $\rightarrow$ 1 is exhibited. The second perturbation energies result of the various interacting NBOs exposed very important  $n \rightarrow \sigma^*$ ,  $n \rightarrow \pi^*$ ,  $\pi \rightarrow n^*$  and  $\pi \rightarrow \pi^*$  types of interaction between natural orbitals around the cluster structures, contributing to total stabilization energies. Though, no significant inter-fragment stabilization interactions occurred between NBOs of fragments. We conclude that the formation of clusters of H<sub>2</sub>O on quinoline, cinnoline, quinazoline and quinoxaline is possible but non-spontaneous, but little aqueous chemistry is predictable.

**Table 9.** Results from the second order perturbation theory analysis performed with Gaussian 09 for all clusters studied with DFT/B3LYP method and 631-G (d) basis set.

Donor	Occupancy	Acceptor	Occupancy	E (2) Kcal/mol	E(j)-E(i) a.u.	F (j,i) a.u.
<b>QNOL1</b>						
$\pi$ C1 - C2	1.72237	$\pi^*$ C3 - C4	0.45392	14.45	0.29	0.061
		$\pi^*$ C5 - N16	0.31039	25.11	0.27	0.075
$\pi$ C3 - C4	1.52055	$\pi^*$ C1 - C2	0.23661	18.47	0.27	0.067
		$\pi^*$ C5 - N16	0.31039	14.61	0.25	0.056
		$\pi^*$ C9 - C12	0.24845	16.13	0.28	0.064
		$\pi^*$ C10 - C11	0.23232	14.53	0.29	0.062
$\pi$ C5 - N16	1.80242	$\pi^*$ C1 - C2	0.23661	10.84	0.34	0.055
		$\pi^*$ C3 - C4	0.45392	18.70	0.34	0.076
$\pi$ C9 - C12	1.74010	$\pi^*$ C3 - C4	0.45392	16.55	0.28	0.064
		$\pi^*$ C10 - C11	0.23232	16.58	0.30	0.063
$\pi$ C10 - C11	1.72058	$\pi^*$ C3 - C4	0.45392	17.85	0.28	0.066
		$\pi^*$ C9 - C12	0.24845	17.90	0.29	0.065
$\pi^*$ C3 - C4	0.45392	$\pi^*$ C9 - C12	0.24845	238.20	0.01	0.077
		$\pi^*$ C10 - C11	0.23232	151.54	0.02	0.079
$\pi^*$ C5 - N16	0.31039	$\pi^*$ C1 - C2	0.23661	114.62	0.02	0.082
		$\pi^*$ C3 - C4	0.45392	135.33	0.02	0.074
<b>QNOL2</b>						
$\pi$ C1 - C2	1.73957	LP (1) C3	1.00879	40.26	0.15	0.087
		$\pi^*$ C5 - C6	0.24062	17.12	0.30	0.064
$\pi$ C5 - C6	1.72983	LP* (1) C4	0.96601	43.15	0.15	0.088
		$\pi^*$ C1 - C2	0.24823	17.42	0.29	0.064
$\pi$ C10 - C14	1.72280	LP (1) C3	1.00879	37.16	0.16	0.086
		$\pi^*$ C13 - N17	0.30197	24.96	0.28	0.075
$\pi$ C13 - N17	1.79733	LP* (1) C4	0.96601	40.26	0.20	0.101
		$\pi^*$ C10 - C14	0.23279	10.87	0.34	0.054
LP (1) C3	1.00879	$\pi^*$ C1 - C2	0.24823	54.35	0.15	0.100
		$\pi^*$ C10 - C14	0.23279	59.05	0.14	0.102
LP* (1) C4	0.96601	$\pi^*$ C5 - C6	0.24062	50.77	0.15	0.011
		$\pi^*$ C13 - N17	0.30197	56.74	0.12	0.093
$\pi^*$ C13 - N17	0.30197	$\pi^*$ C10 - C14	0.23279	125.39	0.02	0.082
<b>QNOL3</b>						
$\pi$ C1 - C2	1.72094	$\pi^*$ C3 - C4	0.45327	15.05	0.29	0.062
		$\pi^*$ C5 - N16	0.29651	24.00	0.28	0.073
$\pi$ C3 - C4	1.52242	$\pi^*$ C1 - C2	0.23081	17.70	0.27	0.066
		$\pi^*$ C5 - N16	0.29651	14.45	0.26	0.057
		$\pi^*$ C9 - C12	0.25240	16.63	0.28	0.064
		$\pi^*$ C10 - C11	0.24246	15.26	0.28	0.062
$\pi$ C5 - N16	1.79061	$\pi^*$ C1 - C2	0.23081	11.58	0.33	0.056
		$\pi^*$ C3 - C4	0.45327	19.48	0.33	0.076
$\pi$ C9 - C12	1.74418	$\pi^*$ C3 - C4	0.45327	16.14	0.29	0.064
		$\pi^*$ C10 - C11	0.24246	16.96	0.30	0.064
$\pi$ C10 - C11	1.73408	$\pi^*$ C3 - C4	0.45327	16.94	0.28	0.065
		$\pi^*$ C9 - C12	0.25240	17.66	0.29	0.064
$\sigma$ C12 - H15	1.98272	$\sigma^*$ C3 - C9	0.02223	4.11	1.07	0.059
LP (1) N16	1.92371	$\sigma^*$ C1 - C5	0.02872	10.52	0.87	0.087
		$\sigma^*$ C3 - C4	0.04271	10.58	0.87	0.086
$\pi^*$ C3 - C4	0.45327	$\pi^*$ C10 - C11	0.24246	248.07	0.01	0.079
$\pi^*$ C5 - N16	0.29651	$\pi^*$ C1 - C2	0.23081	131.35	0.02	0.081
		$\pi^*$ C3 - C4	0.45327	219.29	0.01	0.079
<b>QNOL4</b>						
$\pi$ C1 - C2	1.72537	$\pi^*$ C3 - C4	0.45197	14.38	0.29	0.061
		$\pi^*$ C5 - N16	0.29624	24.27	0.28	0.074
$\sigma$ C1 - H7	1.98253	$\sigma^*$ C5 - N16	0.01143	4.06	1.11	0.060
$\pi$ C3 - C4	1.52284	$\pi^*$ C1 - C2	0.23405	18.14	0.27	0.067
		$\pi^*$ C5 - N16	0.29624	14.42	0.26	0.057
		$\pi^*$ C9 - C12	0.24665	16.47	0.28	0.064
		$\pi^*$ C10 - C11	0.24492	15.21	0.28	0.062

(continued on next page)



Table 9 (continued)

Donor	Occupancy	Acceptor	Occupancy	E (2) Kcal/mol	E(j)-E(i) a.u.	F (j,i) a.u.
$\pi$ C5 – N16	1.79140	$\pi^*$ C1 – C2	0.23405	11.39	0.33	0.055
		$\pi^*$ C3 – C4	0.45197	19.41	0.33	0.076
$\pi$ C9 – C12	1.73835	$\pi^*$ C3 – C4	0.45197	16.11	0.28	0.064
		$\pi^*$ C10 – C11	0.24492	17.49	0.29	0.064
$\pi$ C10 – C11	1.73596	$\pi^*$ C3 – C4	0.45197	16.99	0.23	0.065
		$\pi^*$ C9 – C12	0.24665	17.13	0.29	0.064
LP (1) N16	1.92350	$\sigma^*$ C1 – C5	0.02899	10.54	0.87	0.086
		$\sigma^*$ C3 – C4	0.04244	10.50	0.87	0.086
$\pi^*$ C5 – N16	0.29624	$\pi^*$ C1 – C2	0.23405	142.15	0.02	0.080
		$\pi^*$ C3 – C4	0.45197	197.30	0.01	0.075
<b>CNOL2</b>						
$\pi$ C1 – C2	1.73877	LP (1) C3	0.97922	42.49	0.15	0.089
$\pi$ C1 – C2	1.73877	$\pi^*$ C5 – C6	0.21735	15.68	0.30	0.062
$\sigma$ C2 – H9	1.98148	$\sigma^*$ C3 – C4	0.04221	4.22	1.06	0.060
$\pi$ C5 – C6	1.73199	LP* (1) C4	0.97587	41.56	0.15	0.086
		$\pi^*$ C1 – C2	0.22920	17.76	0.29	0.065
$\sigma$ H7 – C10	1.98116	$\sigma^*$ C13 – N16	0.03000	4.53	1.03	0.061
$\pi$ C10 – C13	1.67309	LP (1) C3	0.97922	45.81	0.15	0.091
		$\pi^*$ N15 – N16	0.39966	23.30	0.24	0.068
$\sigma$ C13 – H14	1.97964	$\pi^*$ N15 – N16	0.39966	5.48	1.03	0.067
$\pi$ N15 – N16	1.80908	LP* (1) C4	0.97587	28.99	0.22	0.092
LP (1) C3	0.97922	$\pi^*$ C10 – C13	0.23329	16.25	0.37	0.070
		$\pi^*$ C1 – C2	0.22920	49.96	0.15	0.098
LP* (1) C4	0.97587	$\pi^*$ C10 – C13	0.23329	54.43	0.14	0.101
		$\pi^*$ C5 – C6	0.21735	48.61	0.15	0.099
LP (1) N15	1.93896	$\pi^*$ N15 – N16	0.39966	112.98	0.09	0.107
		$\sigma^*$ C3 – C4	0.04221	10.34	0.89	0.086
LP (1) N16	1.91904	$\pi^*$ C13 – N16	0.03000	10.33	0.86	0.085
		$\sigma^*$ C4 – N15	0.03336	10.17	0.86	0.084
$\pi^*$ N15 – N16	0.39966	$\pi^*$ C10 – C13	0.23329	45.45	0.06	0.080
<b>CNOL3</b>						
$\pi$ C1 – C2	1.73879	LP (1) C3	0.97921	42.49	0.15	0.089
		$\pi^*$ C5 – C6	0.21731	15.68	0.30	0.062
$\sigma$ C1 – H8	1.98247	$\sigma^*$ C2 – C3	0.02297	4.19	1.07	0.060
$\pi$ C5 – C6	1.73202	LP* (1) C4	0.97585	41.56	0.15	0.086
		$\pi^*$ C1 – C2	0.22915	17.76	0.29	0.065
$\pi$ C10 – C13	1.73202	LP (1) C3	0.97921	45.83	0.15	0.091
		$\pi^*$ N15 – N16	0.39981	23.31	0.24	0.068
$\pi$ N15 – N16	1.80902	LP* (1) C4	0.97585	29.00	0.22	0.092
		$\pi^*$ C10 – C13	0.23338	16.26	0.37	0.070
LP (1) C3	0.97921	$\pi^*$ C1 – C2	0.22915	49.95	0.15	0.098
		$\pi^*$ C10 – C13	0.23338	54.45	0.14	0.101
LP* (1) C4	0.97585	$\pi^*$ C5 – C6	0.21731	48.60	0.15	0.099
		$\pi^*$ N15 – N16	0.39981	113.06	0.09	0.107
LP (1) N15	1.93896	$\sigma^*$ C3 – C4	0.04221	10.34	0.89	0.086
		$\sigma^*$ C13 – N16	0.03000	10.32	0.86	0.085
LP (1) N16	1.91896	$\sigma^*$ C4 – N15	0.03335	10.17	0.86	0.084
$\pi^*$ N15 – N16	0.39981	$\pi^*$ C10 – C13	0.23338	45.47	0.06	0.080
<b>CNOL4</b>						
$\pi$ C1 – C2	1.73816	$\pi^*$ C3 – C4	0.45387	16.88	0.29	0.065
		$\pi^*$ C5 – C6	0.22457	16.30	0.30	0.063
$\sigma$ C1 – H8	1.98280	$\sigma^*$ C2 – C3	0.02301	4.12	1.07	0.059
$\sigma$ C2 – H9	1.98057	$\sigma^*$ C3 – C4	0.04209	4.29	1.06	0.060
$\pi$ C3 – C4	1.50306	$\pi^*$ C1 – C2	0.22824	14.76	0.28	0.062
		$\pi^*$ C5 – C6	0.22457	14.88	0.28	0.062
		$\pi^*$ C10 – C13	0.23666	16.62	0.28	0.065
		$\pi^*$ N15 – N16	0.38100	23.33	0.23	0.067
$\pi$ C5 – C6	1.73793	$\pi^*$ C1 – C2	0.22824	17.28	0.29	0.064
		$\pi^*$ C3 – C4	0.45387	16.33	0.28	0.064

(continued on next page)



Table 9 (continued)

Donor	Occupancy	Acceptor	Occupancy	E (2) Kcal/mol	E(j)-E(i) a.u.	F (j,i) a.u.
$\pi$ C10 – C13	1.68207	$\pi^*$ C3 – C4	0.45387	16.38	0.29	0.064
		$\pi^*$ N15 – N16	0.38100	23.54	0.25	0.069
$\pi$ N15 – N16	1.80166	$\pi^*$ C3 – C4	0.45387	15.18	0.35	0.070
		$\pi^*$ C10 – C13	0.23666	16.21	0.36	0.069
LP (1) N15	1.94001	$\sigma^*$ C3 – C4	0.04209	10.40	0.89	0.086
		$\sigma^*$ C13 – N16	0.02945	10.07	0.86	0.084
LP (1) N16	1.94235	$\sigma^*$ C4 – N15	0.03511	10.54	0.85	0.085
$\pi^*$ C3 – C4	0.45387	$\pi^*$ C5 – C6	0.22457	224.61	0.01	0.078
$\pi^*$ N15 – N16	0.38100	$\pi^*$ C3 – C4	0.45387	76.02	0.04	0.081
		$\pi^*$ C10 – C13	0.23666	50.37	0.05	0.080
<b>QNAZ2</b>						
$\pi$ C1 – C2	1.73107	LP (1) C3	1.02311	40.84	0.15	0.087
		$\pi^*$ C5 – C6	0.23261	17.59	0.30	0.065
$\sigma$ C1 – H8	1.98256	$\sigma^*$ C2 – C3	0.02248	4.05	1.07	0.059
$\sigma$ C1 – H9	1.97508	$\sigma^*$ C3 – C4	0.04072	4.31	1.06	0.061
$\pi$ C5 – C6		LP* (1) C4	0.94559	46.20	0.14	0.089
		$\pi^*$ C1 – C2	0.23865	16.64	0.29	0.063
$\pi$ C10 – N16	1.72004	LP (1) C3	1.02311	23.05	0.19	0.076
		$\pi^*$ C13 – N15	0.27606	29.38	0.32	0.087
$\pi$ C13 – N15	1.79101	LP* (1) C4	0.94559	43.16	0.20	0.104
		$\pi^*$ C10 – N16	0.26562	8.97	0.32	0.049
LP (1) C3	1.02311	$\pi^*$ C1 – C2	0.23865	54.20	0.15	0.101
		$\pi^*$ C10 – N16	0.26562	79.51	0.13	0.111
LP* (1) 4	0.94559	$\pi^*$ C5 – C6	0.23261	48.50	0.15	0.099
		$\pi^*$ C13 – N15	0.27606	49.94	0.12	0.090
LP (1) N15	1.90080	$\sigma^*$ C13 – N16	0.03394	12.30	0.85	0.093
LP (1) N16	1.92323	$\sigma^*$ C3 – C10	0.03426	10.60	0.88	0.087
		$\sigma^*$ C13 – N15	0.01123	11.62	0.91	0.093
<b>QNAZ3</b>						
$\pi$ C1 – C2	1.73081	LP (1) C3	1.02277	40.79	0.15	0.087
		$\pi^*$ C5 – C6	0.23039	17.49	0.30	0.065
$\sigma$ C2 – H8	1.98148	$\sigma^*$ C3 – C4	0.04245	4.33	1.06	0.061
$\pi$ C5 – C6	1.71924	LP* (1) C4	0.94422	45.72	0.15	0.089
		$\pi^*$ C1 – C2	0.23718	16.68	0.29	0.063
$\pi$ N11 – C12	1.98980	LP* (1) C4	0.94422	43.53	0.20	0.103
		$\pi^*$ N14 – C15	0.27897	9.46	0.31	0.049
$\pi$ N14 – C15	1.77511	LP (1) C3	1.02277	21.59	0.20	0.075
		$\pi^*$ N11 – C12	0.26636	27.91	0.33	0.086
LP (1) C3	1.02277	$\pi^*$ C1 – C2	0.23718	53.99	0.15	0.101
		$\pi^*$ N14 – C15	0.27897	86.29	0.12	0.113
LP* (1) C4	0.94422	$\pi^*$ C5 – C6	0.23039	48.41	0.15	0.099
		$\pi^*$ N11 – C12	0.26636	50.44	0.13	0.091
LP (1) N11	1.91819	$\sigma^*$ C3 – C4	0.02258	10.23	0.87	0.085
		$\sigma^*$ C12 – N14	0.03826	13.51	0.83	0.096
LP (1) N14	1.90903	$\sigma^*$ C3 – C15	0.03272	9.62	0.89	0.084
		$\sigma^*$ N11 – C12	0.02411	10.84	0.92	0.091
		$\sigma^*$ O17 – H19	1.99824	9.20	0.85	0.080
<b>QNAZ4</b>						
$\pi$ C1 – C2	1.72813	$\pi^*$ C3 – C4	0.44611	16.16	0.28	0.063
		$\pi^*$ C5 – C6	0.23643	17.99	0.29	0.065
$\sigma$ C2 – H9	1.98056	$\sigma^*$ C3 – C4	0.04195	4.41	1.06	0.061
$\pi$ C3 – C4	1.52256	$\pi^*$ C1 – C2	0.23591	16.69	0.28	0.065
		$\pi^*$ C5 – C6	0.23643	13.99	0.28	0.060
		$\pi^*$ C10 – N16	0.26875	25.36	0.26	0.076
		$\pi^*$ C13 – N15	0.27018	12.49	0.26	0.054
$\pi$ C5 – C6	1.72548	$\pi^*$ C1 – C2	0.23591	16.33	0.29	0.062
		$\pi^*$ C3 – C4	0.44611	18.42	0.28	0.067
$\pi$ C10 – N16	1.76831	$\pi^*$ C3 – C4	0.44611	9.67	0.33	0.054
		$\pi^*$ C13 – N15	0.27018	28.27	0.32	0.086

(continued on next page)

Table 9 (continued)

Donor	Occupancy	Acceptor	Occupancy	E (2) Kcal/mol	E(j)-E(i) a.u.	F (j,i) a.u.
$\pi$ C13 – N15	1.78563	$\pi^*$ C3 – C4	0.44611	20.70	0.33	0.079
		$\pi^*$ C10 – N16	0.01144	9.43	0.32	0.050
LP (1) N15	1.91942	$\sigma^*$ C3 – C4	0.04195	10.11	0.88	0.085
		$\sigma^*$ C13 – N16	0.03669	13.43	0.83	0.095
LP (1) N16	1.92572	$\sigma^*$ C3 – C10	0.03407	10.42	0.88	0.086
		$\sigma^*$ C13 – N15	0.02601	11.45	0.92	0.093
$\pi^*$ C3 – C4	0.04195	$\pi^*$ C1 – C2	0.23591	234.45	0.01	0.077
		$\pi^*$ C5 – C6	0.23643	247.84	0.01	0.079
$\pi^*$ C10 – N16	0.26875	$\pi^*$ C3 – C4	0.44611	213.43	0.01	0.081
$\pi^*$ C13 – N15	0.27018	$\pi^*$ C3 – C4	0.44611	225.26	0.01	0.074
<b>QNOX2</b>						
$\pi$ C1 – C2	1.72706	LP (1) C3	0.97636	44.14	0.14	0.088
		$\pi^*$ C5 – C6	0.23909	17.35	0.29	0.064
$\sigma$ C2 – H8	1.98041	$\sigma^*$ C3 – C4	0.04996	4.34	1.04	0.060
$\pi$ C5 – C6	1.72873	LP* (1) C4	0.97411	44.91	0.14	0.088
		$\pi^*$ C1 – C2	0.23546	16.85	0.30	0.064
$\sigma$ C11 – H12	1.98225	$\sigma^*$ C3 – N19	0.02212	5.08	1.03	0.065
$\pi$ C11 – N19	1.77335	LP (1) C3	0.97636	39.76	0.20	0.100
		$\pi^*$ N13 – C17	0.27948	16.64	0.31	0.065
$\pi$ N13 – C17	1.78621	LP* (1) C4	0.97411	39.07	0.20	0.100
		$\pi^*$ C11 – N19	0.26772	14.82	0.32	0.063
LP (1) C3	0.97636	$\pi^*$ C1 – C2	0.23546	49.46	0.15	0.100
		$\pi^*$ C11 – N19	0.26772	59.17	0.12	0.096
LP* (1) C4	0.97411	$\pi^*$ C5 – C6	0.23909	49.47	0.15	0.100
		$\pi^*$ N13 – C17	0.27948	59.19	0.12	0.094
LP (1) N13	1.90854	$\sigma^*$ C3 – C4	0.04996	9.48	0.88	0.082
LP (1) N19	1.92659	$\sigma^*$ C3 – C4	0.04996	10.12	0.87	0.084
		$\sigma^*$ C11 – C17	0.03855	10.14	0.87	0.085
<b>QNOX3</b>						
$\pi$ C1 – C2	1.72877	LP* (1) C3	0.97413	44.91	0.14	0.088
		$\pi^*$ C5 – C6	0.23539	16.84	0.30	0.064
$\sigma$ C2 – H8	1.98054	$\sigma^*$ C3 – C4	0.04996	4.34	1.04	0.060
$\pi$ C5 – C6	1.72711	LP (1) C4	0.97635	44.13	0.14	0.088
		$\pi^*$ C1 – C2	0.23901	17.35	0.29	0.064
$\pi$ C11 – N15	1.77333	LP (1) C4	0.97635	39.77	0.20	0.100
		$\pi^*$ C12 – N16	0.27955	16.64	0.31	0.065
$\pi$ C12 – N16	1.78619	LP* (1) C3	0.97413	39.06	0.20	0.100
		$\pi^*$ C11 – N15	0.26778	14.83	0.32	0.063
LP* (1) C3	0.97413	$\pi^*$ C1 – C2	0.23901	49.44	0.15	0.100
		$\pi^*$ C12 – N16	0.27955	59.21	0.12	0.094
LP (1) 4	0.97635	$\pi^*$ C5 – C6	0.23539	49.44	0.15	0.100
		$\pi^*$ C11 – N15	0.26778	59.18	0.12	0.096
LP (1) N15	1.92660	$\sigma^*$ C3 – C4	0.04996	10.12	0.87	0.084
		$\sigma^*$ C11 – H12	0.03854	10.14	0.87	0.085
<b>QNOX4</b>						
$\pi$ C1 – C2	1.71899	LP* (1) C3	0.97467	46.54	0.14	0.088
		$\pi^*$ C5 – C6	0.01314	17.34	0.29	0.064
$\sigma$ C1 – H7	1.98254	$\sigma^*$ C2 – C3	0.02416	4.06	1.07	0.059
$\pi$ C5 – C6	1.72734	LP (1) C4	0.97492	44.90	0.14	0.088
		$\pi^*$ C1 – C2	0.22984	16.73	0.30	0.064
$\pi$ C11 – N19	1.79101	LP* (1) C3	0.97467	37.45	0.20	0.100
		$\pi^*$ N13 – C17	0.27222	14.81	0.33	0.063
$\pi$ N13 – C17	1.77284	LP (1) C4	0.97492	39.43	0.20	0.100
		$\pi^*$ C11 – N19	0.29012	16.73	0.31	0.065
LP* (1) C3	0.97467	$\pi^*$ C1 – C2	0.22984	47.54	0.16	0.100
		$\pi^*$ C11 – N19	0.29012	62.59	0.11	0.095
LP (1) C4	0.97492	$\pi^*$ C5 – C6	0.01314	48.69	0.15	0.099
		$\pi^*$ N13 – C17	0.27222	60.81	0.12	0.097
LP (1) N13	1.92617	$\sigma^*$ C3 – C4	0.04970	10.11	0.87	0.084
		$\sigma^*$ C11 – C17	0.03812	10.19	0.87	0.085

## Declarations

### Author contribution statement

Obieze C. Enudi: Performed the experiments; Analyzed and interpreted the data; Wrote the paper.

Hitler Louis: Conceived and designed the experiments.

Moses M. Edim, John A. Agwupuye, Francis O. Ekpen: Contributed reagents, materials, analysis tools or data.

Emmanuel A. Bisong, Patrick M. Utsu: Contributed reagents, materials, analysis tools or data; Wrote the paper.

### Funding statement

This research did not receive any specific grant from funding agencies in the public, commercial, or not-for-profit sectors.

### Data availability statement

Data will be made available on request.

### Declaration of interests statement

The authors declare no conflict of interest.

### Additional information

No additional information is available for this paper.

## Acknowledgements

The authors wish to acknowledge the Computational Chemistry and Bio-simulation Research group leader, Hitler Louis for designing and supervising this research. Obieze C. Enudi is also grateful to his PI, Moses M. Edim, for his undisputed input to the success of this project.

## References

- J. Kumari, Application of heterocyclic compounds in everyday life, *J. Mod. Chem. Chem. Technol.* 9 (1) (2018) 1–7.
- T. Fei, P. Lv, Y. Liu, C. He, C. Sun, S. Pang, Design and synthesis of a series of CL-20 cocrystals: six-membered symmetrical N-heterocyclic compounds as effective cofomers, *Cryst. Growth Des.* 19 (5) (2019) 2779–2784.
- A. Shaabani, M.T. Nazeri, R. Afshari, 5-Amino-pyrazoles: potent reagents in organic and medicinal synthesis, *Mol. Divers.* 23 (3) (2019) 751–807.
- A. De Oliveira Silva, J. McQuade, M. Szostak, Recent advances in the synthesis and reactivity of isothiazoles, *Adv. Synth. Catal.* 361 (13) (2019) 3050–3067.
- V.S. De Andrade, M.C. de Mattos, N-halo reagents: modern synthetic approaches for heterocyclic synthesis, *Synthesis* 51 (9) (2019) 1841–1870.
- S.Y. Atanasova-Stamova, S.F. Georgieva, M.B. Georgieva, Reaction strategies for synthesis of imidazole derivatives: a review, *Scripta Scientifica Pharmaceutica* 5 (2) (2018) 7–13.
- K.P. Kapri, S.B. Singar, S. Khanal, B. Shakya, Synthesis of schiff bases of 4-amino-5-(2-hydroxyphenyl)-4H-1, 2, 4-triazole-3-thiol as potent antimicrobial agents, *Amrit Res. J.* 1 (1) (2020) 29–36.
- R. Budhwan, G. Garg, I.N. Namboothiri, S. Murarka, Hypervalent iodine (III) reagents in the synthesis of heterocyclic compounds, *Targets Heterocycl. Syst.* 20 (2020) 27–52.
- F. Ferlin, L. Luciani, O. Viteritti, F. Brunori, O. Piermatti, S. Santoro, L. Vaccaro, Polarclean as a sustainable reaction medium for the waste minimized synthesis of heterocyclic compounds, *Front. Chem.* 6 (2019) 659.
- S.K. Ahmed, W.B. Ali, A.A. Khadom, Synthesis and investigations of heterocyclic compounds as corrosion inhibitors for mild steel in hydrochloric acid, *Int. J. Ind. Chem.* 10 (2) (2019) 159–173.
- C. Cabrele, O. Reiser, The modern face of synthetic heterocyclic chemistry, *J. Org. Chem.* 81 (21) (2016) 10109–10125.
- M.M. Edim, O.C. Enudi, B.B. Asuquo, H. Louis, E.A. Bisong, J.A. Agwupuye, F.I. Basse, Aromaticity indices, electronic structural properties, and fuzzy atomic space investigations of naphthalene and its aza-derivatives, *Heliyon* 7 (2) (2021), e06138.
- A. Vidal-Vidal, O.N. Faza, C. Silva Lopez, CO<sub>2</sub> complexes with five-membered heterocycles: structure, topology, and spectroscopic characterization, *J. Phys. Chem.* 121 (47) (2017) 9118–9130.
- J. Ren, J. Li, J. Li, Z. Chen, F. Cheng, Tracking multiple aromatic compounds in a full-scale coking wastewater reclamation plant: interaction with biological and advanced treatments, *Chemosphere* 222 (2019) 431–439.
- E.Y. Tyunina, V.G. Badelin, I.N. Mezhevoi, Observation of complex formation between L-histidine and heterocyclic compounds in water and aqueous buffer solution using calorimetric and spectroscopic methods, *J. Mol. Liq.* 278 (2019) 505–511.
- Bamdad, H., Papari, S., MacQuarrie, S., & Hawboldt, K. Study of surface heterogeneity and nitrogen functionalizing of biochars: molecular modeling approach. *Carbon*, 171, 161-170.
- Á.V. Vidal, C.S. López, O.N. Faza, Nitrogen doped nano hoops as promising CO<sub>2</sub> capturing devices, *Phys. Chem. Chem. Phys.* 20 (13) (2018) 8607–8615.
- D. Prieschl, G. Belanger-Chabot, X. Guo, M. Dietz, M. Muller, I. Krummenacher, H. Braunschweig, Synthesis of complex boron–nitrogen heterocycles comprising borylated triazines and tetrazenes under mild conditions, *J. Am. Chem. Soc.* 142 (2) (2019) 1065–1076.
- L.Y. Xie, T.G. Fang, J.X. Tan, B. Zhang, Z. Cao, L.H. Yang, W.M. He, Visible-light-induced deoxygenative C2-sulfonylation of quinoline N-oxides with sulfinic acids, *Green Chem.* 21 (14) (2019) 3858–3863.
- J. Zhang, C. Zheng, M. Zhang, Y. Qiu, Q. Xu, W.C. Cheong, D. Wang, Controlling N-doping type in carbon to boost single-atom site Cu catalyzed transfer hydrogenation of quinoline, *Nano Res.* 13 (11) (2020) 3082–3087.
- M. Szumilak, A. Stanczak, Cinnoline scaffold—a molecular heart of medicinal chemistry? *Molecules* 24 (12) (2019) 2271.
- A.S. El-Azab, A.M. Alaa, S. Bua, A. Nocentini, M.A. El-Gendy, M.A. Mohamed, C.T. Supuran, Synthesis of benzenesulfonamides linked to quinazoline scaffolds as novel carbonic anhydrase inhibitors, *Bioorg. Chem.* 87 (2019) 78–90.
- Z. Wang, H. Li, Z. Peng, Z. Wang, Y. Wang, P. Lu, Preparation and photophysical properties of quinazoline-based fluorophores, *RSC Adv.* 10 (51) (2020) 30297–30303.
- M. Montana, F. Mathias, T. Terme, P. Vanelle, Antitumoral activity of quinoxaline derivatives: a systematic review, *Eur. J. Med. Chem.* 163 (2019) 136–147.
- M.P. Evangelin, T.S. Gold, Y. Elisha, G. Radhika, G.K. Vamsi, K. Arathi, A concise review on cinnolines, *Innovat. J. Med. Health Sci.* 10 (4) (2020) 897–901.
- Shruti Varshney, V. Saxena, Design, synthesis, characterization and biological evaluation of some novel cinnolo piperazine derivatives, *Int. J. Pharm. Pharmaceut. Sci.* 6 (2014) 245–248.
- G. Zoidis, A. Sosic, S. Da Ros, B. Gatto, C. Sissi, F., Palluotto, M. Catto, Indenocinnoline derivatives as G-quadruplex binders, topoisomerase II $\alpha$  inhibitors and antiproliferative agents, *Bioorg. Med. Chem.* 25 (9) (2017) 2625–2634.
- E.D. Awad, M.M. El-Abadelah, S. Matar, M.A. Zihlif, R.G. Naffa, E.Q. Al-Momani, M.S. Mubarak, Synthesis and biological activity of some 3-(4-(Substituted)-piperazin-1-yl) cinnolines, *Molecules* 17 (1) (2012) 227–239.
- I.M. Khan, K. Alam, M.J. Alam, M. Ahmad, Spectrophotometric and photocatalytic studies of H-bonded charge transfer complex of oxalic acid with imidazole: single crystal XRD, experimental and DFT/TD-DFT studies, *New J. Chem.* 43 (23) (2019) 9039–9051.
- R. Kavitha, S. Nirmala, R. Nithyabalaji, R. Sribalan, Biological evaluation, molecular docking and DFT studies of charge transfer complexes of quinaldic acid with heterocyclic carboxylic acid, *J. Mol. Struct.* 1204 (2020) 127508.
- X. Zhang, J. Chen, G. Lou, J. Li, F. Wang, Theoretical prediction of new structure, mechanical properties, anisotropy in elasticity and thermodynamic properties of Mo<sub>3</sub>Ge material, *Vacuum* 170 (2019) 108978.
- S.E. Adeniji, G.A. Shallangwa, D.E. Arthur, M. Abdullahi, A.Y. Mahmoud, A. Haruna, Quantum modelling and molecular docking evaluation of some selected quinoline derivatives as anti-tubercular agents, *Heliyon* 6 (3) (2020), e03639.
- N. Flores-Holguín, J. Frau, D. Glossman-Mitnik, Chemical reactivity and bioactivity properties of the Phallotoxin family of fungal peptides based on Conceptual Peptidology and DFT study, *Heliyon* 5 (8) (2019), e02335.
- C. Verma, M.A. Quraishi, E.E. Ebenso, Quinoline and its derivatives as corrosion inhibitors: a review, *Surface. Interfac.* (2020) 100634.
- Z.M. Alamshany, A.A. Ganash, Synthesis, characterization, and anti-corrosion properties of an 8-hydroxyquinoline derivative, *Heliyon* 5 (11) (2019), e02895.
- N. Uludağ, G. Serdaroglu, New route for synthesis of 2-(2, 2-dimethoxyethyl)-1, 2, 3, 4, 5, 6-hexahydro-1, 5-methanoazocino [4, 3-b] indole and DFT investigation, *Heliyon* 6 (6) (2020), e04105.
- T. Sasitha, W.J. John, Design, docking, and DFT investigations of 2, 6-bis (3, 4-dihydroxyphenyl)-3-phenethylpiperidin-4-one, *Heliyon* 7 (2) (2021), e06127.
- O. Hurtado-Aular, A.B. Vidal, J. Peña-Mena, A. Sierraalta, R. Añez, DFT thermodynamic study of the adsorption of CO<sub>2</sub> and H<sub>2</sub>O on W<sub>3</sub>O<sub>x</sub>/M (1 1 1)(x= 6 or 9 and M= Cu, Ag or Au). Insight for the water-gas shift reaction, *Appl. Surf. Sci.* 531 (2020) 147337.
- C. Caglioti, F. Palazzetti, Potential energy surfaces for water interacting with diatomic heteronuclear molecules: H<sub>2</sub>O–HF as a case study, *Chem. Phys. Lett.* (2021) 138692.
- I. Warad, S. Musameh, I. Badran, N.N. Nassar, P. Brandao, C.J. Tavares, A. Barakat, Synthesis, solvatochromism and crystal structure of trans-[Cu (Et<sub>2</sub>NCH<sub>2</sub>CH<sub>2</sub>NH<sub>2</sub>)<sub>2</sub> H<sub>2</sub>O](NO<sub>3</sub>)<sub>2</sub> complex: experimental with DFT combination, *J. Mol. Struct.* 1148 (2017) 328–338.
- S. Carlotto, L. Pandolfo, M. Casarin, Trinuclear Cu (II) complexes from the classic [Cu<sub>2</sub>(RCOO)<sub>4</sub>(H<sub>2</sub>O)<sub>2</sub>] lantern complex and pyrazole: a DFT modelling of the reaction path, *Inorg. Chim. Acta.* 470 (2018) 93–99.
- M. Centanni, D.J.A. Moes, I.F. Trocóniz, J. Ciccolini, J.C. van Hasselt, Clinical pharmacokinetics and pharmacodynamics of immune checkpoint inhibitors, *Clin. Pharmacokinet.* (2019) 1–23.

- [43] J.W.C. Alfenaar, T. Gumbo, K.E. Dooley, C.A. Peloquin, H. McIlerron, A.. Zagorski, G.B. Migliori, Integrating pharmacokinetics and pharmacodynamics in operational research to end tuberculosis, *Clin. Infect. Dis.* 70 (8) (2020) 1774–1780.
- [44] G.W. Trucks, M.J. Frisch, H.B. Schlegel, G.E. Scuseria, M.A. Robb, J.R. Cheeseman, G. Scalmani, V. Barone, B. Mennucci, G.A. Petersson, H. Nakatsuji, M. Caricato, X. Li, H.P. Hratchian, A.F. Izmaylov, J. Bloino, G. Zheng, J.L. Sonnenberg, M. Hada, M. Ehara, K. Toyota, R. Fukuda, J. Hasegawa, M. Ishida, T. Nakajima, Y. Honda, O. Kitao, H. Nakai, T. Vreven, J.A. Montgomery, J.E. Peralta Jr., F. Ogliaro, M. Bearpark, J.J. Heyd, E. Brothers, K.N. Kudin, V.N. Staroverov, R. Kobayashi, J. Normand, K. Raghavachari, A. Rendell, J.C. Burant, S.S. Iyengar, J. Tomasi, M. Cossi, N. Rega, J.M. Millam, M. Klene, J.E. Knox, J.B. Cross, V. Bakken, C. Adamo, J. Jaramillo, R. Gomperts, R.E. Stratmann, O. Yazyev, A.J. Austin, R. Cammi, C. Pomelli, J.W. Ochterski, R.L. Martin, K. Morokuma, V.G. Zakrzewski, G.A. Voth, P. Salvador, J.J. Dannenberg, S. Dapprich, A.D. Daniels, O. Farkas, J.B. Foresman, J.V. Ortiz, J. Cioslowski and D.J. Fox, Gaussian09, Revision D. 01, Gaussian, Inc., Wallingford CT, 2013.
- [45] T. Scior, H.H. Abdallah, K. Salvador-Atonal, S. Laufer, Dapsone is not a pharmacodynamic lead compound for its aryl derivatives, *Curr. Comput. Aided Drug Des.* 16 (3) (2020) 327–339.
- [46] Lu. Tian, Chen. Feiwu, Multiwfn: a multifunctional analyzer, *J. Comput. Chem.* 33 (5) (2012) 580–592.
- [47] S. Emamian, T. Lu, H. Kruse, H. Emamian, Exploring nature and predicting strength of hydrogen bonds: a correlation analysis between atoms-in-molecules descriptors, binding energies, and energy components of symmetry-adapted perturbation theory, *J. Comput. Chem.* 40 (32) (2019) 2868–2881.
- [48] J.G. Brandenburg, S. Grimme, Accurate modeling of organic molecular crystals by dispersion-corrected density functional tight binding (DFTB), *J. Phys. Chem. Lett.* 5 (11) (2014) 1785–1789.
- [49] Meng Xiao, Tian Lu, Generalized charge decomposition analysis (GCDA) method, *J. Adv. Phys. Chem.* 4 (2015) 111–124.
- [50] S. Emamian, T. Lu, H. Kruse, H. Emamian, Exploring nature and predicting strength of hydrogen bonds: a correlation analysis between atoms-in-molecules descriptors, binding energies, and energy components of symmetry-adapted perturbation theory, *J. Comput. Chem.* 40 (32) (2019) 2868–2881.
- [51] G. Mierzwa, A.J. Gordon, S. Berski, Topological analysis of electron localisation function: unlocking the nature of BC chemical bond. Possible existence of multiple bonds BC and BC, *Polyhedron* 170 (2019) 180–187.
- [52] J.W. Ochterski, *Thermochemistry in Gaussian 1*, Gaussian Inc, 2000, p. 19.
- [53] J. Zhao, A. Khalizov, R. Zhang, R. McGraw, Hydrogen-bonding interaction in molecular complexes and clusters of aerosol nucleation precursors, *J. Phys. Chem.* 113 (4) (2009) 680–689.
- [54] C. Xie, D. Yan, W. Chen, Y. Zou, R. Chen, S., Zang, S. Wang, Insight into the design of defect electrocatalysts: from electronic structure to adsorption energy, *Mater. Today* 31 (2019) 47–68.
- [55] Y. Mao, M. Head-Gordon, Probing blue-shifting hydrogen bonds with adiabatic energy decomposition analysis, *J. Phys. Chem. Lett.* 10 (14) (2019) 3899–3905.
- [56] O.A. Stasyuk, R. Sedlak, C.F. Guerra, P. Hobza, Comparison of the DFT-SAPT and canonical EDA schemes for the energy decomposition of various types of noncovalent interactions, *J. Chem. Theor. Comput.* 14 (7) (2018) 3440–3450.
- [57] S. Sadeghi, H.M. Shiri, A. Ehsani, M. Oftadeh, Electrosynthesis of high-purity TbMn2O5 nanoparticles and its nanocomposite with conjugated polymer: surface, density of state and electrochemical investigation, *Solid State Sciences*, 2020, p. 106227.
- [58] M. Barborini, S. Sorella, M. Rontani, S. Corni, Correlation effects in scanning tunneling microscopy images of molecules revealed by quantum Monte Carlo, *J. Chem. Theor. Comput.* 12 (11) (2016) 5339–5349.
- [59] Ying Zhu, Hongbin Chen, Phenylalanine system fragment CDA and orbital interaction, *J. Jilin Univ. (Sci. Ed.)* 57 (1) (2019) 145–150.
- [60] T. Lu, S. Manzetti, Wavefunction and reactivity study of benzo [a] pyrene diol epoxide and its enantiomeric forms, *Struct. Chem.* 25 (5) (2014) 1521–1533.
- [61] S. Emamian, T. Lu, H. Kruse, H. Emamian, Exploring nature and predicting strength of hydrogen bonds: a correlation analysis between atoms-in-molecules descriptors, binding energies, and energy components of symmetry-adapted perturbation theory, *J. Comput. Chem.* 40 (32) (2019) 2868–2881.
- [62] S. Shahbazian, Why bond critical points are not “bond” critical points, *Chem. A Eur. J.* 24 (21) (2018) 5401–5405.
- [63] S. Noorizadeh, E. Shakerzadeh, Shannon entropy as a new measure of aromaticity, Shannon aromaticity, *Phys. Chem. Chem. Phys.* 12 (18) (2010) 4742–4749.
- [64] A. Matrodi, S. Noorizadeh, N-Derivatives of Shannon entropy density as response functions, *Phys. Chem. Chem. Phys.* 22 (37) (2020) 21535–21542.
- [65] I.R. Gould, I.H. Hillier, Solvation of alanine dipeptide: a quantum mechanical treatment, *J. Chem. Soc., Chem. Commun.* (11) (1993) 951–952.
- [66] L.C. Allen, D.A. Egolf, E.T. Knight, C. Liang, Bond polarity index, *J. Phys. Chem.* 94 (14) (1990) 5602–5607.
- [67] A.S. Ghasemi, M.R. Taghartapeh, A. Soltani, P.J. Mahon, Adsorption behavior of metformin drug on boron nitride fullerenes: thermodynamics and DFT studies, *J. Mol. Liq.* 275 (2019) 955–967.
- [68] K. Bamba, O.W. Patrice, N. Ziao, NBO population analysis and electronic calculation of four azopyridine ruthenium complexes by DFT method, *Comput. Chem.* 5 (1) (2017) 51.
- [69] N. Günay, Ö. Tamer, D. Kuzalic, D. Avci, Y. Atalay, Theoretical investigation of N-methyl-N'-(4-nitrobenzylidene) pyrazine-2-carbohydrazide: conformational study, NBO analysis, molecular structure and NMR spectra, *Acta Phys. Pol., A* 127 (3) (2015).